Fluorescent Probes in Cellulo Recognitions of Alkaline Phosphatases

Subjects: Chemistry, Analytical

Contributor: Madhusudan Dasnur Nanjappa, Anup Pandith, Svetlana Sankaran, Dorothy Priyanka Dorairaj, Anusha Anjaneya Reddy, Hari Prasad Badubanahalli Ramesh

Alkaline phosphatase (ALP) is one of the vital phospho-ester bond cleaving biocatalysts that has inevitable significance in cellular systems, viz., early-stage osteoblast differentiation, cell integrity in tissues, bone mineralization, cancer biomarker, liver dysfunction, cellular osmotic pressure, protein folding and many more. Variation from optimal levels of ALP in intra and extracellular fluids can cause severe diseases, including death. Due to these reasons, ALP is considered as a vital biomarker for various preclinical and medical diagnosis. Fluorescence image-based diagnosis is the most widely used method, owing to its simplicity, robustness, non-invasive properties and excellent spatio-temporal resolution (up to the nM/pM level), as compared to conventional analytical techniques, such as the electroanalytical method, nuclear magnetic resonance (NMR) and high-performance liquid chromatography (HPLC). Most of the reviews reported for ALP's recognition in the literature scarcely explain the structurally related, photophysical and biophysical parameters; and the sub-cellular localizations. Considering these facts, in order to enhance the opto-analytical parameters of fluorescence-based diagnostic materials at the cellular level, herein we have systematically documented recent developments in the opto-analytical capabilities of quencher-free probes for ALP, used in in vitro (biological buffers) to in cellulo conditions, along with in vivo models.

Keywords: Alkaline phosphatase (ALP) ; Fluorescent probes ; Intramolecular charge transfer ; Photoinduced charge transfer ; Two photon fluorescence ; Nuclear magnetic resonance

1. Introduction

Alkaline phosphatase (ALP) is the vital Zn containing glycoprotein, generally expressed on the cell membrane and utilized for the hydrolysis of phosphorylated organic/inorganic molecules preferably at neutral to basic pH levels [1]. ALP molecular weight generally falls between 70,000 and 200,000 Da with an isoelectric point range from pH 5.4 to 6.0, and shows a high hydrolysis rate at pH 8–9 (weak alkaline conditions) [2]. Most of the biologically originated phosphorylated molecules, such as nucleotides, alkaloids and proteins, can be dephosphorylated in the presence of ALP [3]. ALP belongs to one of the *ectophosphatase* (kinase/phosphatase) enzymes, which generally control the extra and intracellular phosphates' homeostasis in cells and tissues, and have significant roles in embryogenesis, bone mineralization, vascular calcification, terminiotoxin detoxification, inflammatory responses and neuronal functions [4][5]. Deviations from the optimal level of ALP in serum can lead several diseases, such as hepatitis [6]; prostate, ovarian and breast cancers [7]; bone cancer [8]; diabetes [9][10]; Paget's disease [11]; bile duct obstruction [12]; blood malignancies [13]; leukemia; and Wilson's disease [14]. Due to these reasons; ALP is regarded as an important indicator in clinical and medical diagnostics [15][16][17]. Recently, it has been found that children and pregnant women's sera have as much as 500 U/L of ALP [18]. In contrast, normal healthy adults can show 35–160 U/L of ALP in their sera [19], depending on age and other biological factors.

ALP can be found in liver, kidney, bone, intestinal epithelium, lung, leukocytes and placental cells [20]. Depending on the origin, ALPs are classified as intestinal ALP (*intestinal absorption*), placental ALP, bone (mineralization) ALP, germ cell ALP, blood ALP (usually originating from chromosome **1**) and tissue-non-specific ALPs (generally originating from chromosome **2**). Irrespective of their origin, almost all ALPs typically exhibit common physiological properties in different locations.

In general, mammalian ALPs are zinc-containing metalloenzymes, functioning as dimeric biomacromolecules bearing two Zn^{2+} and one Mg^{2+} in their active sites [21][22]. Apparently, the two Zn ions are separated by approximately 4.0 A° units, bound by His331, His412, Asp327, Asp369 and His370 amino-acid residues [23]. Asp51's carboxylate group can act as a bridge connecting Zn and Mg ions. Usually, pyrophosphates (PPi) are encapsulated in the pocket of the two Zn ions and additionally stabilized through the hydrogen bonding with guanidinium units of Arg166 residues [24][25][26]. Thermodynamically favorable nucleophilic attack of serine 102 (pK_a 5.50) on the phosphorous center of the PPi-bound complex, in the active center, is the driving force for the phosphate-ester hydrolysis (Scheme 1). It is worth mentioning that Zn and Mg ions are vital metal ions responsible for proper biocatalytic activity of ALP, generally operating through the synergistic regulations between the two active subunits. ALPs can be found in both prokaryotes and eukaryotic cell lines; however, due to the higher significance of mammalian ALPs in biological systems, such as cellular signal transductions, cell division, cell differentiation and bone calcification, in the current review we highlight only mammalian ALPs and their in cellulo recognition, along with in vivo[27][28] models based on fluorescence (bioimaging) methods.

Based on ALP's wide distributions in biological systems, such as in saliva, urine, synovial and cerebrospinal fluids, ALP is considered a vital biomarker in medical diagnostics. [29][30]. Therefore, recognition of ALPs either in intra or extracellular fluids and in tissues with a rapid and accurate method is currently in high demand in biomedical science. Hence, various bioanalytical tools have been used for the recognition of ALPs in in cellulo and in vitro models, such as electro-analytical methods [31][32][33][34], surface enhanced Raman scattering [35][36], Northern blotting [37][38], enzyme linked immunosorbent assay (ELISA) [39], radioimmuno assays [40][41], quartz crystal microbalance [42][43], field effects transistors (FET) [44], colorimetry [45][46][47], magnetic resonance imaging [48] and fluorescence methods [49]. Amongst them, fluorescence methods are considered as far superior owing to their simplicity, cost-effectiveness and high-spatio temporal resolution at the molecular level [50][51][52]. In the last decade, various research groups throughout the globe have actively been involved in the development of novel fluorogenic probes for ALP recognition in both in vitro and in vivo models [53][54].

2. Conceptual Strategies for the Design of ALP Fluorescent Probes in Cellulo Recognition

Most ALP recognition strategies rely on *turn-on* methods of optical responses in biological fluids. It is one of the essential criteria for ideal biomolecular probes, which trigger significant *switch on* responses upon interactions with specific analytes in physiological conditions. Selective recognition capabilities of rationally designed probes, either in chemo-dosimetric (non-reversible, chemical changes) or reversible (non-covalently held) types, substantially induce perturbation in the electronic/rotational/translational energy levels of fluorescent units. There are several photophysical properties that have been documented in the literature, such as photoinduced electron transfer (PET), excited state intramolecular proton transfer (ESIPT), intramolecular charge transfer (ICT), C=N isomerization inhibitions, twisted intramolecular charge transfer (TICT) and aggregated induced emission (AIE) mechanisms, which were exploited in the design of various types of ALP probes [55][56][57][58].

It is evident that most of the reported ALP probes specially designed for cell imaging studies are constructed based on conjugations of fluorescent reporters (fluorophore part), linkers and receptor units. Linkers usually help to hold the fluorophore moiety and receptor unit together without causing steric hindrance in the biocatalytic reaction site. Additionally, receptors (for phosphatase its *phosphoester link*) help to recognize the biocatalytic reaction sites within the biomolecules in question. Pertaining to the conjoining of these concepts, various ALP probes have been designed through the conjugation of fluorescent cores with phosphoester moieties either directly (without linker) or indirectly (with linker). Given the size of a fluorophore, in order to avoid steric hindrance at the dephosphorylation reaction site, most fluorescent reporters have been constructed with a structurally flexible linker. To achieve the best site-specific diagnostics, sometimes ALP probes are associated with targeting components/functional groups. Depending the requirements, subcellular localization (mitochondria, lysosome, endoplasmic reticulum, etc.) of probes will be regulated by incorporating conventional or non-classical targeting functional groups. The photophysical properties of the designed fluorescent materials depend on core unit, substituents and molecular geometry. Conventionally, symmetric and asymmetric molecular structures substantially regulate the photophysical properties of the fluorophoric units through the cumulative dipole moments of each bond, along with their transitional frequencies (energies) within the molecules. With careful consideration of these facts, various fluorescent probes with peculiar absorption and emission behavior have been designed to recognize biomolecules. Differently, based on a complexation and decomplexation strategy, metal complexes have been used to detect ALP activity [59][60][61][62]. In this strategy, ALP is indirectly monitored based on the PPi concentration in in vitro digestion assay protocols. Initially, PPi selective fluorescent ligand-metal complexes are prepared; then, metal ions are extruded from the fluorescent ligands by the sequential addition of PPi ions. Eventually, the optical properties of the fluorescent ligand are regulated based on complexation and decomplexation processes in a sequential manner. Upon performing the PPi digestion in the presence of ALP, the residual amount of PPi in the reaction mixture is monitored. Residual PPi in the reaction mixture for ALP activity has been monitored through opto-analytical methods (UV–Vis and fluorescence methods). It is worth mentioning that most efficient ALP probes are associated with the systematic conjugation of the phosphorylated terminus through the self-immobilized moiety (linkers) to the fluorescent reporter, in association with subcellular organelles targeting functional groups, such as mitochondria, lysosomes and the Golgi apparatus, in a sterically free environment (**Figure 1**). In contrast, indirect methods, such as the use of PPi-regulated organometallic complexes and nano-material-based techniques, could be more effective in in vitro diagnostics rather than in vivo ALP model-based recognition. If these materials are designed rationally, considering site-specific qualitative and quantitative tracking of phosphatase substrates (PPi, nucleotides, etc.), they may provide novel platforms for a future generation of fluorescent materials for ALP activity monitoring based on the indirect approach. Furthermore, this strategy using both the phosphatase and its substrates could be helpful to elucidate the disease states in a biological system at the molecular level.

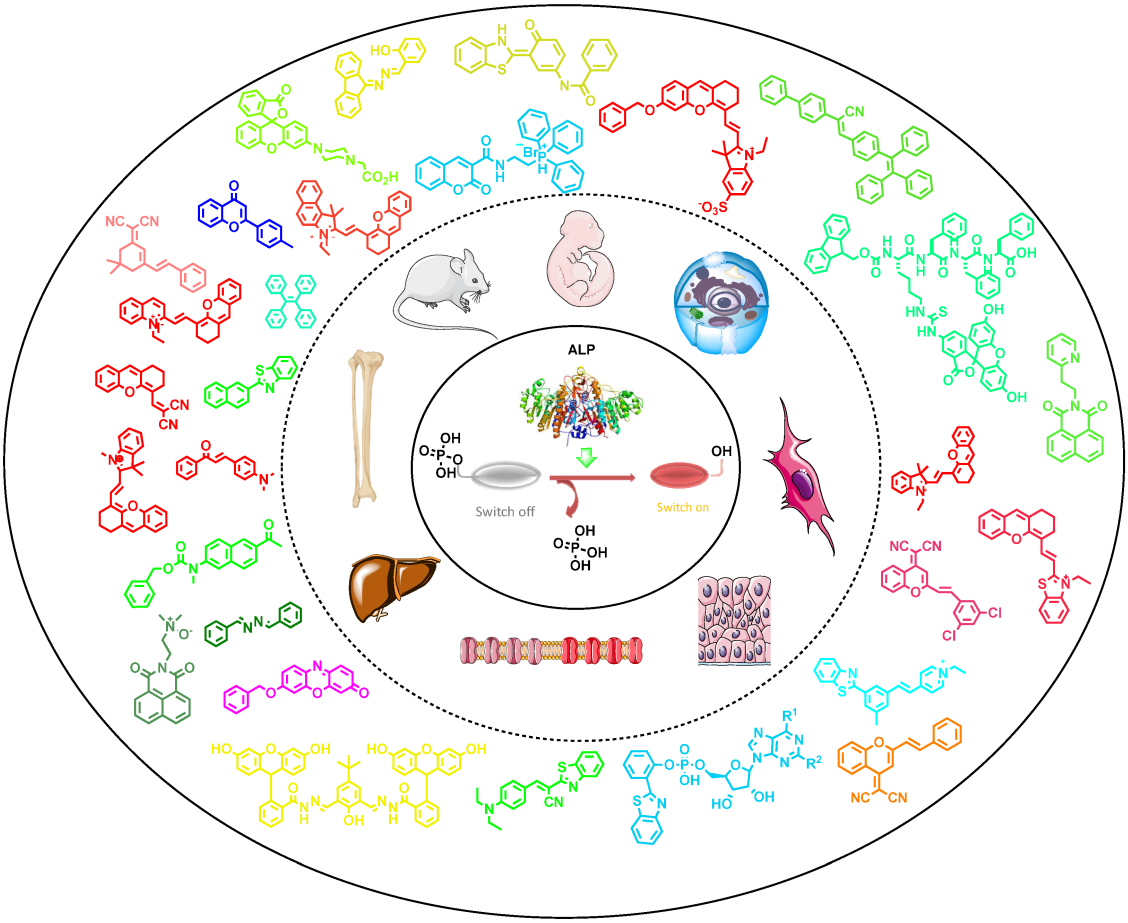

Figure 1. Schematic representation of ALP sensor design strategies for cells, tissues and in vivo models.

3. Small-Molecule-Based Fluorescent Probes

Small molecular probes are always advantageous compared to labelled methods, where biomolecules such as peptides and nucleic acids are generally covalently attached to the fluorophores [63][64][65][66][67]. In this labelling approach, where biomacromolecules are site specifically modified with fluorescent labels, usually suffers from various drawbacks—viz., susceptibility to cellular ions, proteases and nucleases; and always demanding transfecting agents to enter the cells. In contrast, small molecules can enter the cells through passive modes without getting degraded by proteases or nucleases [68][69][70]. Furthermore, small molecules are usually not accompanied by quenching units (such as BHQ) and can have a ability to trigger dual emission (AIE-based materials monomer ↔ excimer) depending on the molecular confinements. Considering these facts, various small molecule based blue/green/red/NIR emissive fluorescent materials were designed for the recognition of ALP.

Zhang et al. reported phosphorylated tetraphenylethylene-based, AIE-based fluorescent probes **ALP-1**, **ALP-2** and **ALP-3** [71] for monitoring of ALPs during osteogenic differentiation of stem cells (**Figure 2**). In these probes, hydrophilicities, were tuned by incorporating mono-, di-, and tetra-phosphate units at the periphery, resulting in a very low quantum yield in aqueous conditions. Probes showed characteristics λ_{max} at ~338 (±4) nm and λ_{em} at 460 (±10) nm in UV–Vis and fluorescence spectra, respectively. In contrast, upon incubation with ALP, the probes showed a turn response within 5 min, at the bluish green region centered at λ_{em} = ~470 nm, which was blue shifted to λ_{em} = ~450 nm after 60 min.

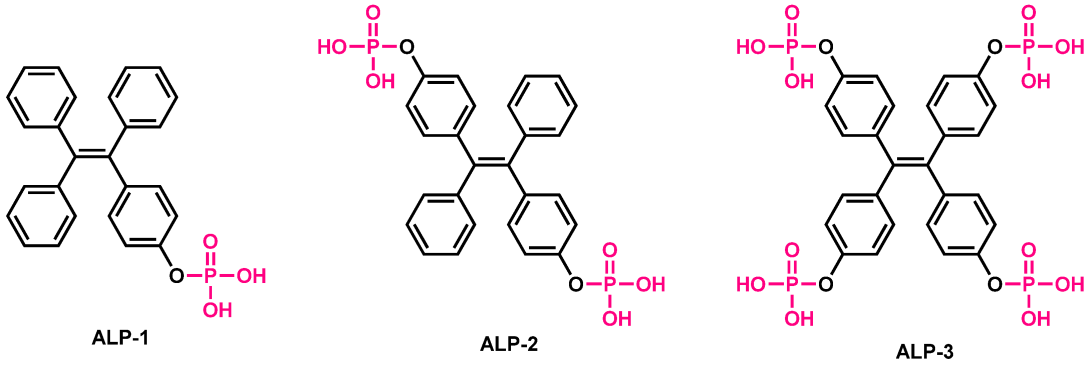

Figure 2. Structure of AIE-based tetraphenylethylene probes **ALP-1**, **ALP-2** and **ALP-3**.

This substantial blue shift, attributed to complete hydrolysis of phosphorylated probes into insoluble hydroxylated tetraphenylethylene units, resulted in highly ordered aggregates. An ALP-regulated *switch on* response was found to be highest in the case of **ALP-2**, followed by **ALP-4** and **ALP-1**, under physiological conditions. In contrast, mono-phosphorylated probe **ALP-1** was found to be very sensitive compared to di- and tetra-phosphorylated probes in similar experimental conditions. The scholars speculate that the presence of multiple phosphorylated units in **ALP-3** induced a complex mechanism of dephosphorylation with ALP, resulting in low sensitivity. Due to these reasons, even though di-phosphorylated probe showed a higher enhancement ratio upon interaction with ALP, the lowest detection limit was found for the mono-phosphorylated probe. Stoichiometrically, at the specified concentration, the mono-phosphorylated probe has quantitatively half of the di-phosphorylated one's units. Only mono- and di-phosphorylated probes were analyzed in biological samples because of their higher sensitivity and stability.

Cytotoxicity studies analyzed through propidium iodide revealed that both **ALP-1** and **ALP-2** can be used effectively at 2 to 20 µM. Upon incubation of 20 µM of probe with **ALP-1/2** during osteogenic differentiation in a bone marrow mesenchymal stem cell (BMSC) culture (0 to 7 days), fluorescence intensities were increased in the green channel, and can be visualized through fluorescence confocal laser scanning microscopic images. Overexpression of ALP during osteogenic differentiation of stem cells was further supported through the flow cytometric Western blotting and rt-PCR analysis. It was found that, in cellular conditions, the di-phosphorylated probe **ALP-2** showed significant changes compared to that of the mono-phosphorylated counterpart.

Upon exploiting the AIE properties in combination with ESIPT behavior, Tang et al. reported a 2′-hydroxychalcone-based phosphorylated probe **ALP-4** (**Figure 3**) for ALP recognition in in vitro and in cellulo [72]. The rationally designed probe triggered far-red emission centered at 640 nm upon ALP-catalyzed dephosphorylation under physiological conditions. **ALP-4** showed absorption maxima at λ_{max} 430 and 416 nm in UV–Vis spectra and weak emission (greenish-yellow λ_{em} 538 nm). This weakly green emissive behavior in the phosphorylated state was attributed to the presence of *N,N,*dimethylaniline and vinyl ketone units, thereby creating an ICT process in the chalcone unit in the twisted conformation. However, upon dephosphorylation, the presence of the ketone unit at the *ortho* position induced strong intramolecular hydrogen bonding upon photochemical excitation, leading to the highly stable 6-membered ring, resulting in keto-enol tautomerism. Based on pH-dependent study, the scholars speculated that fluorescence properties in the probe should be attributed to the combination of synergistic ESIPT and ICT processes. Single crystal analysis of **ALP-4** (**OH**) revealed head-to-head and edge–face stacking resulted in strong intermolecular-coupling-aided AIE behavior. Exploiting such dual photophysical properties in phosphorylated and dephosphorylated 2-hydroxychalcone resulted in ratiometric fluorescence switching properties in green and red channels. The probe detected ALP as scarce as 0.15 mU/mL in a ratiometric manner. The scholars did not specify the kinetic parameters in their work.

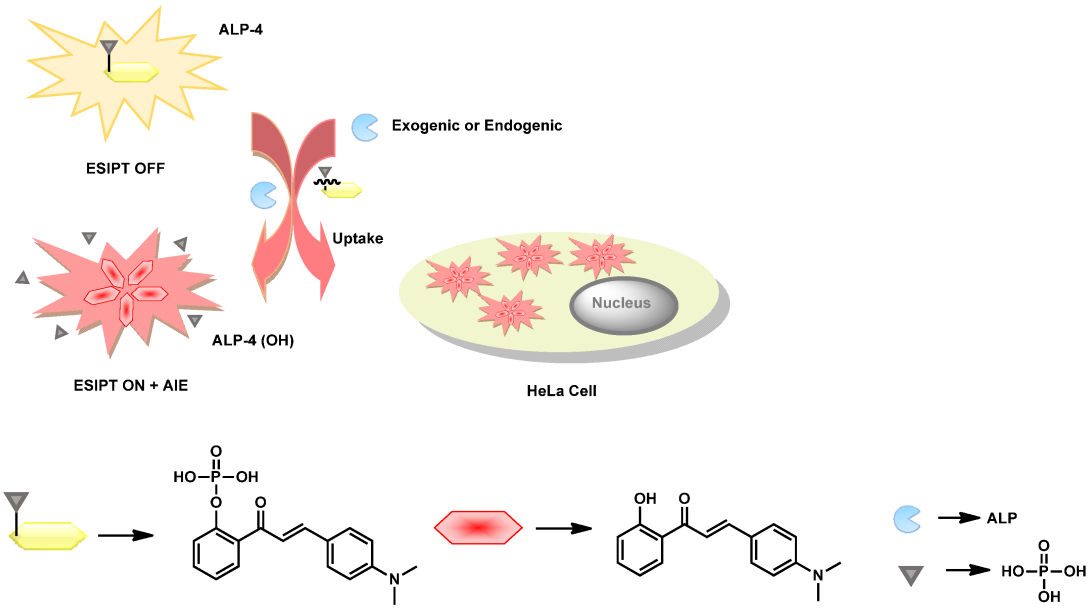

Figure 3. Structure of the ESIPT-AIE-based fluorescent probe **ALP-4** and a plausible phosphatase recognition mechanism.

ALP-4 showed excellent biocompatibility towards HeLa cell lines. Upon incubation of **ALP-4** in endogenously overexpressed HeLa cells, orange fluorescence was seen in the cytoplasm. The scholars speculated on the existence of unusual blue-shifted emission in the orange region in cellular conditions, as compared to that of in vitro conditions (red emissive), could have been due to the twisted molecular confinements of **ALP-4** (**OH**) upon interactions with bio-macromolecules in biological fluids. To validate the intracellular phosphate hydrolysis of **ALP-4**, fluorescence confocal imaging studies (FCIS) were performed in dual channels in the absence and presence of the ALP inhibitor levamisole. According to the results, the scholars postulated that intercellular ALPs readily cleaved the phosphorylated probe in

extracellular fluid, and thereafter the fluorescent **ALP-4** (**OH**) was transfected passively, resulting in bright fluorescence in the cytosol.

Sun et al. and co-workers reported the naphthalene-based green emissive two-photon florescent probe **ALP-5** (**Figure 4**) for in vitro and in cellulo recognition of ALPs [73]. A PO_4^{3-} group was incorporated into the self-cleavable benzyl-ester unit at the ortho position in such a way that, upon dephosphorylation, it could trigger the release of an amino-naphthalene moiety. Under physiological conditions, the probe showed absorption maxima at λ_{max} 300 nm in UV–Vis spectrum and emission maxima centered at λ_{em} 450 nm in the fluorescence spectrum. Upon dephosphorylation in the presence of ALP, the absorption and emission maxima shifted to 365 and 500 nm respectively. Such selective bathochromicity in the absorption spectrum, along with a *switch on* response in the green channel, made the scholars interested in performing ALP recognitions in biological systems.

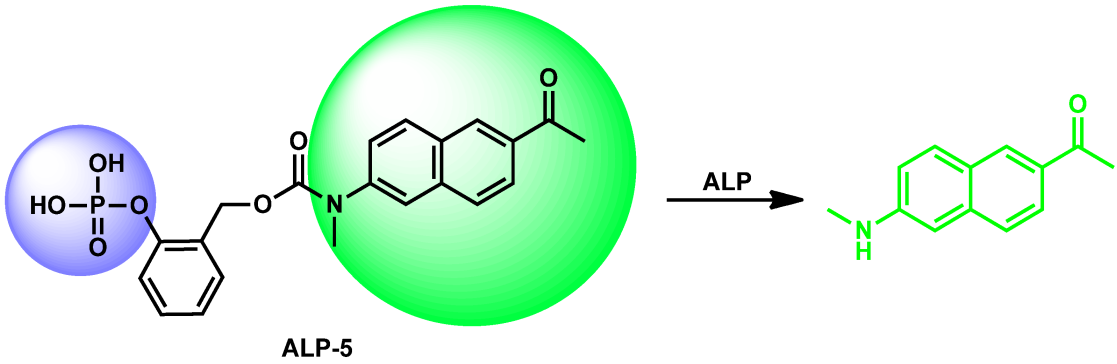

Figure 4. Structure of **ALP-5** probe and a plausible phosphatase mechanism.

Nie et al. developed a new near-infrared, emissive, hemi-cyanin-based fluorescent probe, **ALP-6** (**Figure 5**), for in vitro and in vivo recognition of endogenous ALP activity [74]. **ALP-6** involves phosphorylated chromene units conjugated with benz[e]indolium salts. In buffered conditions, the probe showed an absorption maximum at λ_{max} at 604 nm and was very weakly emissive (λ_{em} 738 nm). Upon incubation with ALP at roughly physiological pH, 8.0, there was a 10-fold enhancement (at 738 nm) in the emission intensity, along with a substantial redshift from 604 to 738 nm in the UV–Vis spectra within 20 min. The designed hemicyanine-based probe showed a highly selective and robust *switch on* response in the NIR region, towards phosphatase, without allowing any interference by biologically relevant ions or macromolecules. The ALP-induced dephosphorylation of **ALP-6** retained a strong ICT process, resulting in high fluorescence with redshifts in the UV–Vis spectrum, which were significantly inhibited by the phosphorylated probe due to the electron pulling effects from the electronegative phosphorous atom in the PO_4^{3-} unit.

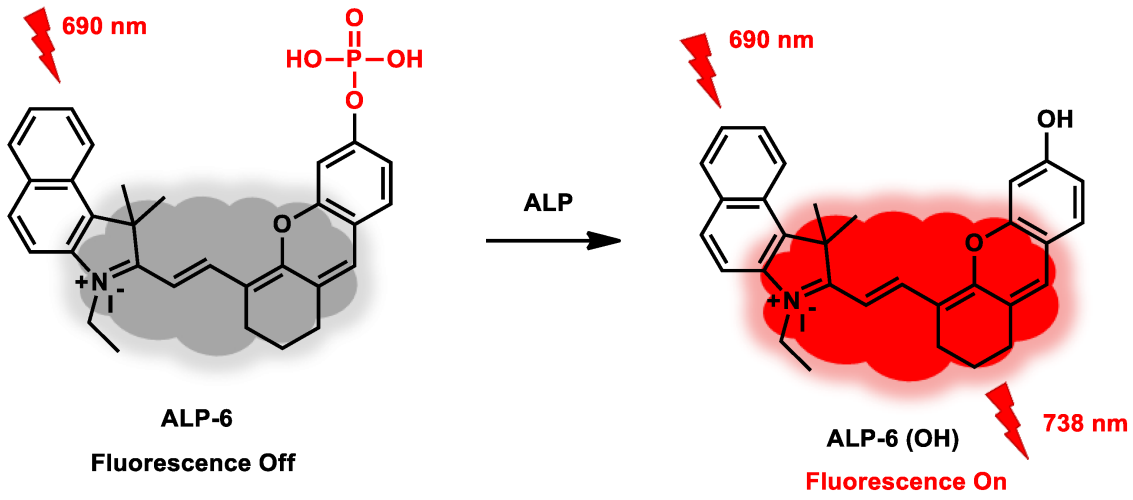

Figure 5. Structure and a plausible phosphatase recognition mechanism of probe **ALP-6**.

Liang's group reported fluorescent peptide **ALP-7 (Figure 6),** for the in vitro recognition of ALP. The designed FITC-conjugated, phosphorylated peptide undergoes dephosphorylation in the presence of ALP, leading to the three-dimensional, self-assembled, fibrous-type material—a "gel" [75] at pH 8.0 (TRIS-HCl). Enzyme-assisted sol to gel transformation resulted in quenching of fluorescence in the green channel attributed to conventional aggregation caused quenching (ACQ). The scholars did not specify kinetic parameters such as V_{max} and K_m. **ALP-7** showed strong green emission upon illumination at 365 nm (UV light), whereas upon incubation with ALP, in physiological pH buffers, a substantial decrement in emission intensity in the green channel was observed. Concomitantly, a significant color change from light green to transparent yellow was clearly seen with the naked eye. Probe was able to recognize ALP as lowest as 0.06 U/mL in similar experimental conditions.

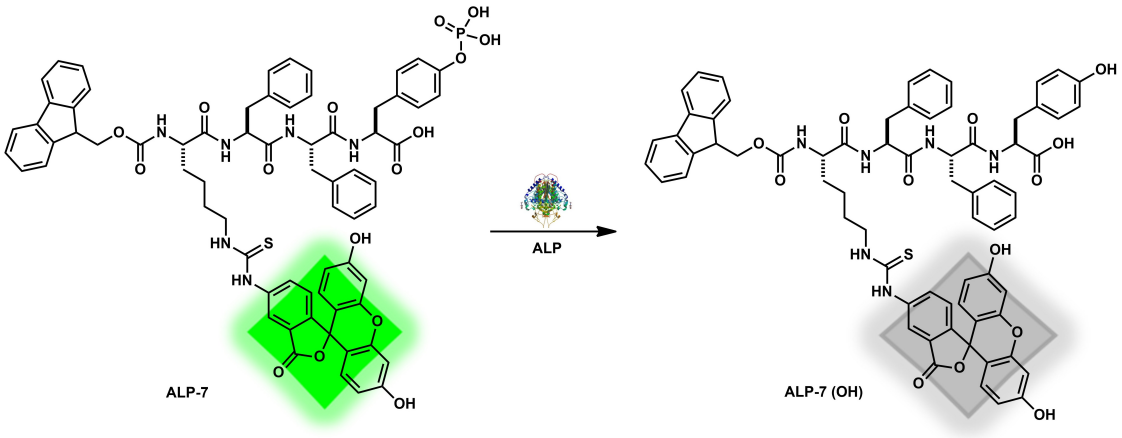

Figure 6. Structure and a plausible phosphatase recognition mechanism of probe **ALP-7**.

Tan et al. reported a hemicyanine-based NIR based fluorescent probe, **ALP-8** (**Figure 7**), for in vitro and in vivo recognition of ALP [76]. In buffered conditions, the probe showed absorption maxima at λ_{max} 600 and 650 nm in the UV–Vis spectrum, and did not induce any fluorescence band in the NIR region. Upon dephosphorylation, absorption maxima λ_{max} were red-shifted to 650 and 680 nm, elicited with bright NIR fluorescence centered at 700 nm. They observed blue shifts in the absorption and emission wavelengths compared to **ALP-6** (benz[e]-indolium core), revealing that indolyl core's conjugation extension can significantly affect the ICT process in hemicyanine-based fluorophore units.

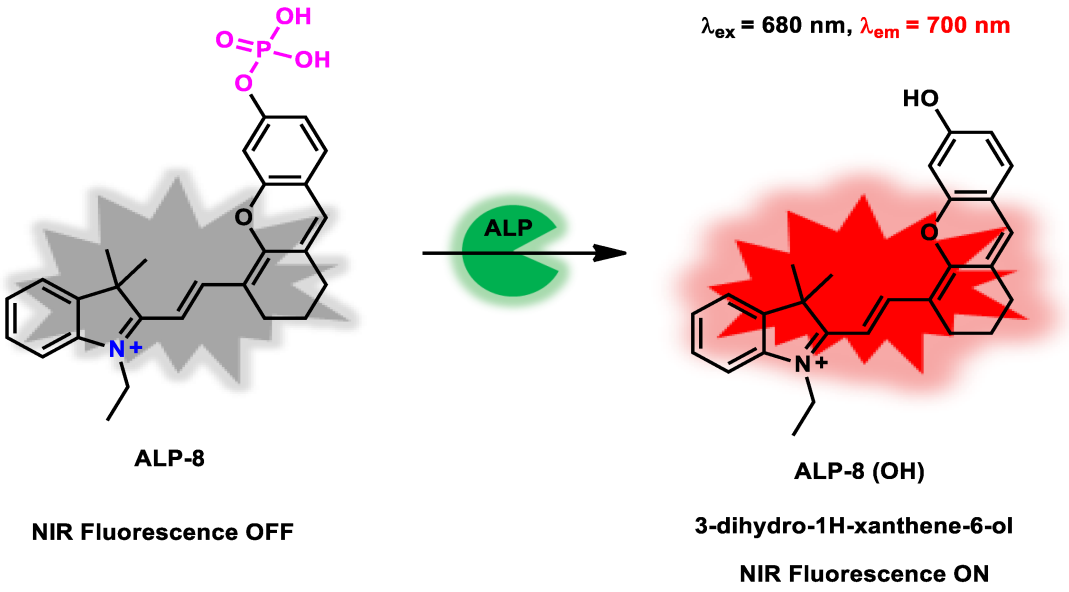

Figure 7. Structure of hemicyanine-based probe **ALP-8** and a plausible phosphatase recognition mechanism.

Wei et al. reported a highly efficient, NIR-regulated far-red probe, **ALP-9** (**Figure 8**) based on the dicyanomethylene-4H-chromene unit conjugated with dichrolorophenyl phosphate ester [77]. To achieve best possible tumor microenvironment (TME) localization and controlled time-resolved intracellular ALP imaging, **ALP-9** was loaded into am NIR-responsive nano-container.

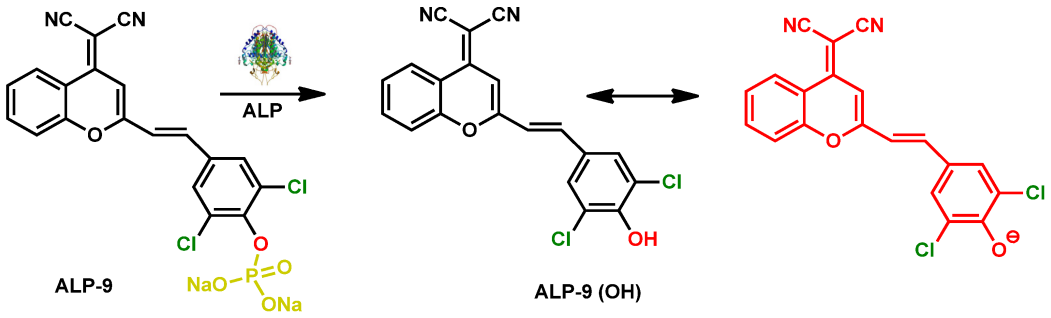

Figure 8. The structure of the NIR-regulated far-red emissive probe **ALP-9** and a plausible phosphatase recognition mechanism in the TME.

Ding et al. reported a novel D–π–A-tuned mitochondria-targeting fluorescence probe (**ALP-10**) whose emission properties are regulated through the ESIPT phenomenon [78]. Molecular engineering was performed by the combination of 2-(2′-hydroxyphenyl)-benzothiazole (ESIPT core) with a 4-styryl-pyridinium (robust mitochondrial targeting unit) core (**Figure 9**). **ALP-10** showed a characteristic broad absorption peak with maximal absorptivity at ca. ~358 nm and an emission maximum at 514 nm (ϕ = 0.21) in UV–Vis and fluorescence spectra, respectively. Upon ALP induced dephosphorylation, the free phenolate unit induced a strong ESIPT process in **ALP-10** (**OH**), resulting in the generation of a new absorption band (λ_{max} ca. ~510 nm) and emission band (λ_{em} ca. ~650 nm). The dephosphorylated product with free phenolic OH emitted a strong red fluorescent signal in a ratiometric manner. The ALP recognition capability of the probe was found to be appreciable in the physiological pH range (5.0 to 8.0). However, at an alkaline pH (pH > 8.0) the ratiometric ALP recognition capability was significantly diminished, which was attributed to inhibition of the ESIPT process pertaining to phenolate ion formation.

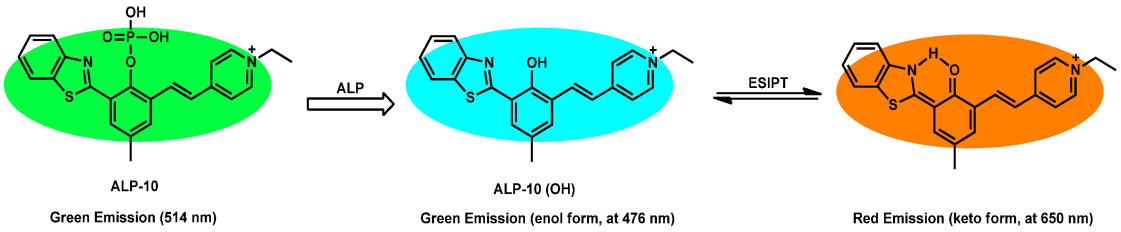

Figure 9. Structure of **ALP-10** and its plausible sensing mechanism for phosphatase.

Han et al. reported the 2′-(2′-hydroxyphenyl)-benzothiazole (HBT) fluorescent conjugates (**Figure 10**) were linked to the 5′ position of the ribonucleoside (adenosine/guanosine) residues for recognition of ALP in cellular conditions [79]. These 5′-ribonucleotide-fluorophore analogues showed weak emission, due to the phosphorylated phenolic OH in HBT unit. P–O bond cleavage (dephosphorylation) generates free HBT and phenolic OH, which exists in a keto–enol tautomerization equilibration. Upon photochemical excitation, the ESIPT core equilibrium shifted toward the enol tautomer (more predominant isomer), resulting in red shifts in the emission spectrum. **ALP-11/12** are non-fluorescent in aqueous buffer, but otherwise have three emission maxima, 370, 375 and 380 nm. Similarly, these probes exhibited a bright fluorescent signal centered at 512 nm in the presence of ALP.

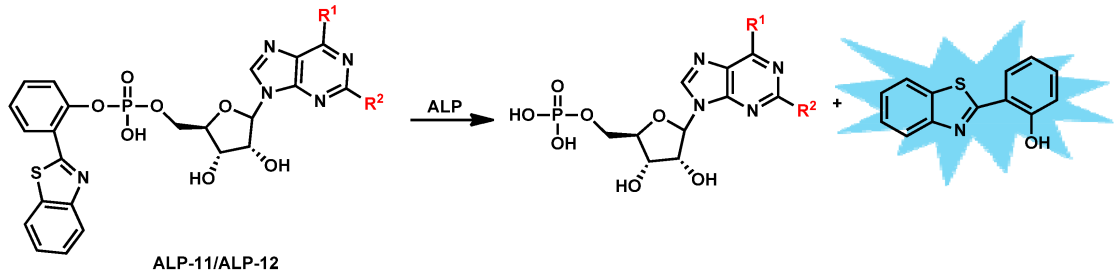

Figure 10. Structures of phosphatase probes **ALP-11** and **ALP-12**. (In **ALP-11**; $R^1 = NH_2$, R^2 = H, **ALP-12**; R^1 = O, $R^2 = NH_2$).

Kim et al. reported a new iminocoumarin-benzothiazole-based fluorophore, **ALP-13** (**Figure 11**) to recognize the phosphatase at the single-cell level [80]. In an aqueous buffer solution, probe showed an absorption maximum of 472 nm and emission maximum (λ_{em}) of 542 nm, in the UV–Vis and fluorescence spectra, respectively.

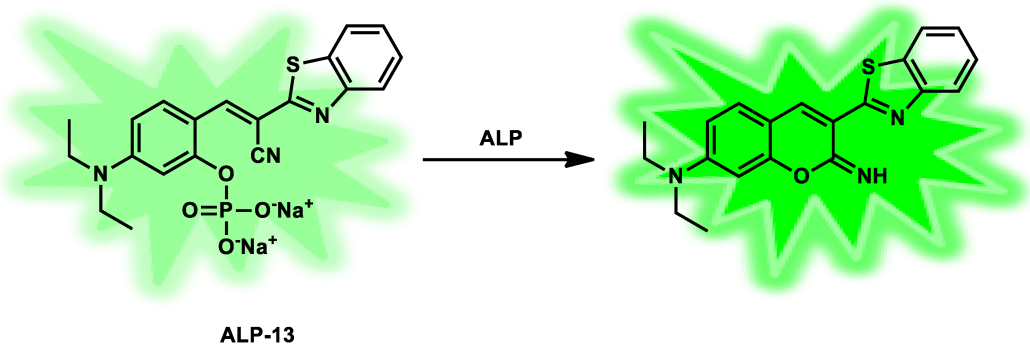

Figure 11. Structure and phosphatase recognition mechanism of iminocoumarin-benzothiazole-based probe **ALP-13**.

Li et al. reported the self-immolative resorufin-based probe **ALP-14** (**Figure 12**) for an ALP assay in cellular conditions [81]. Molecular engineering was performed based on the conjugation of an ALP-recognizing substrate (phosphoester unit) to a red emissive resorufin unit through the reactive *p-hydroxybenzyl* unit, which acts as self-immolative linker. This design is

such that ALP can easily access the phosphor-ester terminus of the probe without steric hindrance, for biocatalytic dephosphorylation. When **ALP-14** is dephosphorylated, it intermediately undergoes 1,6-eliminations to produce a *p*-quinone methide ether derivative and a free *Resorufin* unit. This transformation is associated with changing of the solution's color from orange to purple and generating intense fluorescence emission centered at the 585 nm region.

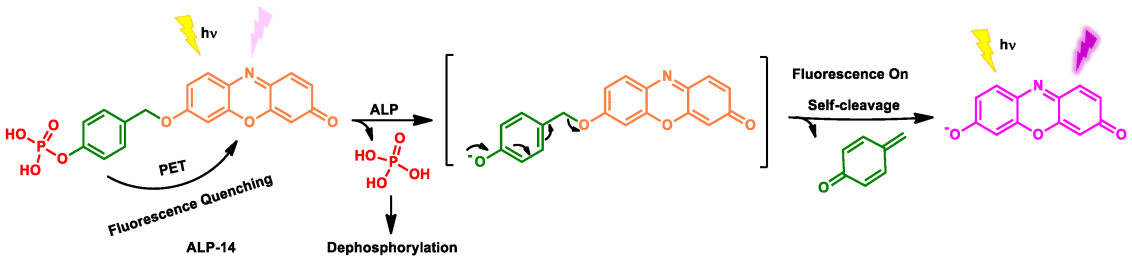

Figure 12. Structure of the self-immolative resorufin-based chromo-fluorescent probe **ALP-14** and a plausible phosphatase recognition mechanism.

Sun et al. reported a novel hydrazone-based fluorescent probe, **ALP-15** (**Figure 13**), for the in cellulo recognition of ALP. The opto-analytical behavior of the probe is regulated through the dual photophysical phenomena, such as aggregation-induced emission (AIE) and excited state intramolecular proton transfer (ESIPT) [82]. The design strategy targeted a simple and small molecular architecture, which showed excellent selectivity and sensitivity, by showing a large Stokes shift upon interacting with phosphatase in physiological conditions.

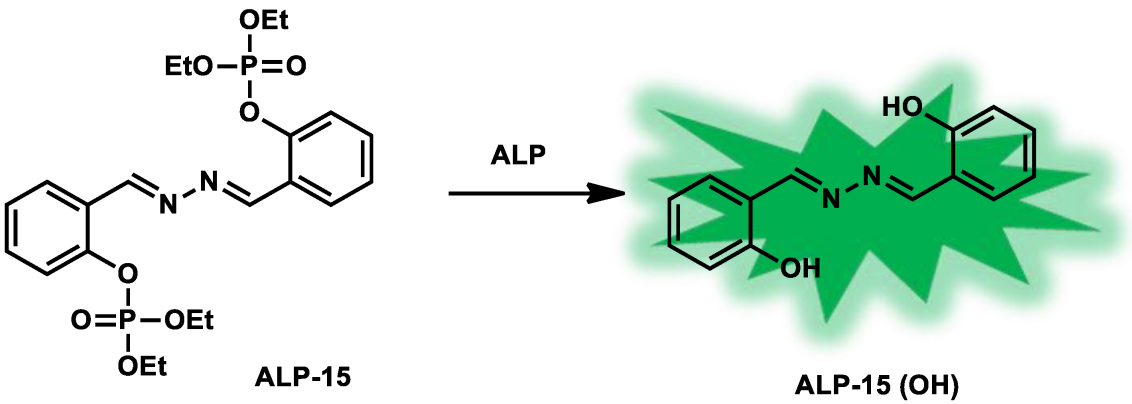

Figure 13. Structure of **ALP-15** and its plausible recognition mechanism with ALP.

Wu et al. developed a 1,8-naphthalimide derivative, **ALP-16**, for real time ratiometric recognition of (**Figure 14**) the organ damage biomarker ALP in cells and in vivo models [83]. A phosphor-ester group was incorporated at the 4th position of the 1,8-naphthalimide core to induce dual emission (blue–green region) and incorporation of a peripheral amine-*N*-oxide group facilitated water solubility and biocompatibility. Upon phosphor-ester hydrolysis, the 4th position of the naphthalimide unit is transformed into free OH. This chemical transformation enormously changes the photophysical properties of the probe, causing a dramatic color change and a ratiometric signal in the emission spectra. In the biological buffer, **ALP-16** exhibited an absorption maximum λ_{max} at ca. ~375 nm, and an emission maximum at λ_{em} 468 nm in the UV–Vis and fluorescence spectra, respectively. Upon ALP-regulated biocatalytic dephosphorylation, electron deficient substituents (phosphoester) were changed to electron donating substituents (phenolic OH) at the 4th position of the 1,8-naphthalimide unit of **ALP-15** (OH). Due to these reasons, significant bathochromic behavior (λ_{max} 375 → 450 nm) was observed in UV–Vis spectra. Similarly, significant ratiometric changes were observed through the concomitant decrement at 468 nm and a significant enhancement at 554 nm (redshift) in the emission signal.

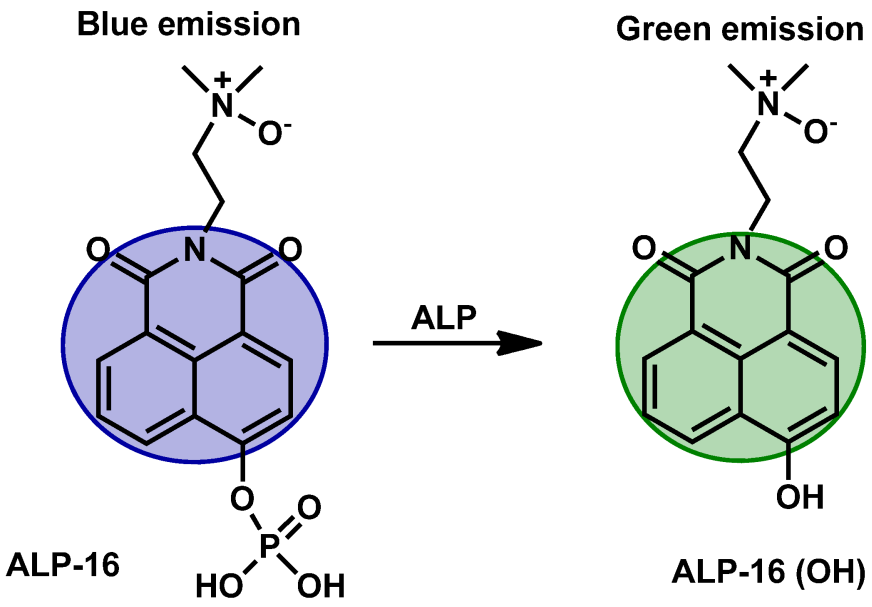

Figure 14. The structure of **ALP-16** and a plausible phosphatase recognition mechanism.

Zhou et al. reported a naphthalene-based two-photon fluorescent probe **ALP-17**[84] for the recognition of ALP (**Figure 15**) in a ratiometric manner. The probe's fluorescence intensity ratio showed a linear relationship with ALP concentration in the range of 20 to 180 U/L, and had a detection limit of 2.3 UL^{-1} in physiological conditions. The scholars did not specify the dephosphorylation kinetic parameters in their work. In a detailed in vitro investigation, **ALP-17** was used to recognize the intracellular ALP activity using one-photon (405 nm) or two-photon (720 nm) excitation techniques. The probe's quantum yield was found to be 0.41. When excited at 720 nm, the probe has a 65 GM two-photon action absorption cross-section at 428 nm. The probe's cytotoxicity was evaluated based on MTT assay in HeLa cells, revealing that **ALP-17** did not have a toxic effect until 20 µM. During incubation with **ALP-17**, HeLa cells exhibited bright green fluorescence after 30 min. In contrast, probe incubated in levamisole-hydrochloride-pre-treated HeLa cells resulted in only blue emission, which supports that **ALP-17** is able to detect intracellular ALP. The probe-incubated HeLa cells resulted in bright fluorescence images upon excitation at λ_{ex} 720 nm, supporting the idea that **ALP-17** is suitable for two-photon imaging as well.

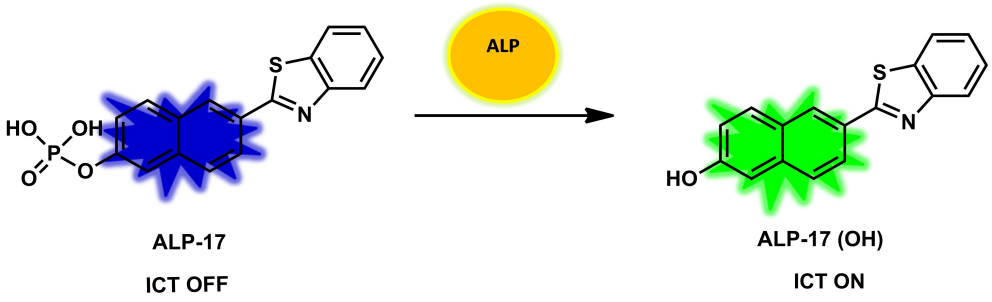

Figure 15. The structure of **ALP-17** and a plausible phosphatase recognition mechanism.

Podder et al. developed the rhodol-based green fluorescent probe **ALP-18** (**Figure 16**), which was used to distinguish cancer cells from normal cells based on lysosomal phosphatase expression [85]. In vitro studies revealed that the probe causes a ~9-fold increment in UV-absorption at λ_{abs} of 490 nm and a ~33-fold emission enhancement at λ_{em} 532 nm in the presence of 1.72 U mL^{-1} of ALP. In this probe, fluorescence emission behavior was tuned through the closed and open structure of the conventional spiro-lactam ring in the rhodol skeleton. In the phosphorylated state, the probe exists in spirocyclic form and exhibited weak fluorescence. However, upon dephosphorylation, the spiro-lactam ring will be opened, resulting in revival of rhodol fluorescence in the green channel. Dephosphorylation kinetic parameters K_M, k_{cat} and k_{cat}/K_M were found to be 7.0 µM, 9.52 s^{-1}, and 13.6 × 10^5 M^{-1} s^{-1}, respectively. The probe did not suffer from interference in the presence of biologically relevant ions and molecules in physiological conditions.

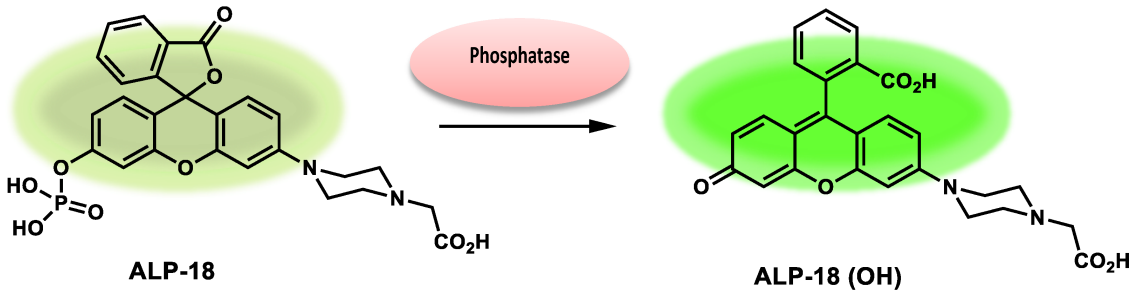

Figure 16. Structure of **ALP-18** and a plausible phosphatase recognition mechanism.

Lu et al. reported ICT tuned dicyano-based fluorogenic substrate (**ALP-19**) for the ratiometric recognition of ALP (**Figure 17**) [86]. The probe showed a significant bathochromic shift (550 → 650 nm) in the emission spectrum, upon biocatalytic dephosphorylation: a substantial color change from yellow-green to light orange. In its phosphorylated state, the probe was weakly emissive due to lowering of electron densities on the phenolic oxygen, which resulted in inhibition of the ICT phenomenon in D–π–A skeleton. However, upon phosphate hydrolysis, phenolic OH enhanced the ICT phenomenon in the probe, resulting in noticeable spectral shifts in the UV–Vis and emission signals. The absorption and emission bands on the probe **ALP-19** exhibited peaks at 440 nm ($\varepsilon = 2.2 \times 10^4\ M^{-1}\ cm^{-1}$) and 550 nm ($\phi = 10.5\%$) respectively. Upon dephosphorylation, a new band appeared at 650 nm ($\phi = 7.5\%$). It is worth noting that due to the weak emission at 650 nm, the dephosphorylated probe exhibited a low quantum yield compared to the phosphorylated form.

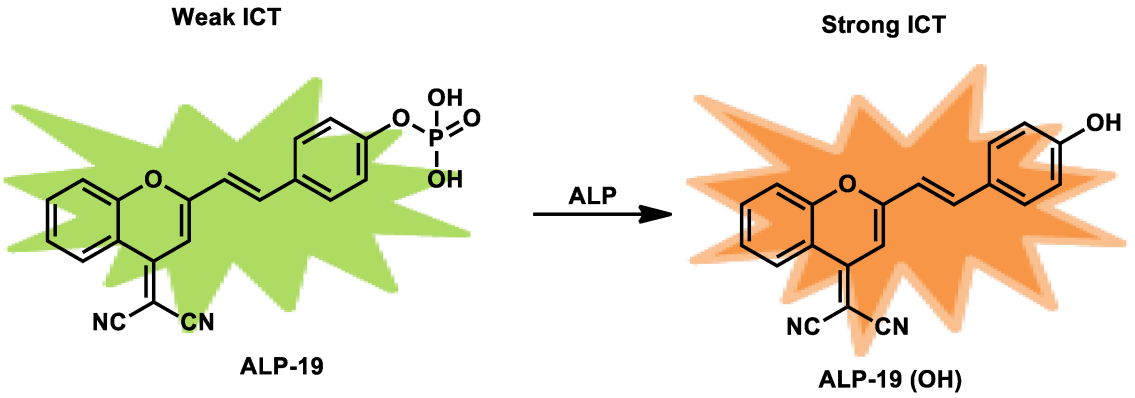

Figure 17. Structure of the far-red emissive dicyano-based fluorescent probe **ALP-19** and a plausible phosphatase recognition mechanism.

Hu et al. reported a new flavone-based fluorescent probe, **ALP-20** (**Figure 18**) (3-hydroxy-2-(p-tolyl)-4H-chromen-4-one), for the in vitro and in cellulo recognition of ALP [87]. Tuning of photophysical behavior in the probe is attributed to inhibition and facilitation of the ESIPT process in phosphorylated and dephosphorylated states, respectively. Due to the presence of a phosphorylated phenolic unit, it is unable to undergo a tautomerization process; as a result, emission intensity is significantly quenched. However, ALP-regulated dephosphorylation induced the keto-enol tautomers through the phenolic OH group, allowing for intensified ESIPT-based emission.

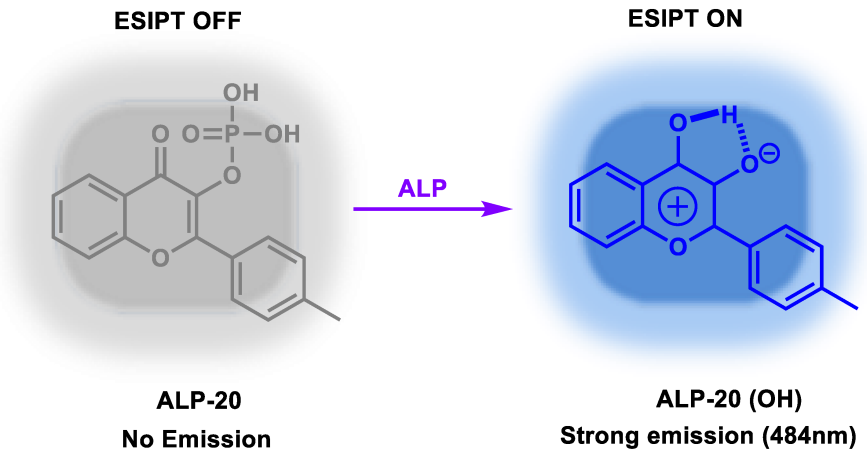

Figure 18. Structure of the flavone-based fluorescent probe **ALP-20** and a plausible phosphatase recognition mechanism.

Liu et al. reported a hemicyanine-based NIR fluorescent probe, **ALP-21** (**Figure 19**), for turn-on trapping of ALP activity in cancer cells and tumor-xenografted nude mouse models [88]. The probe rationale was based on regulation of the intramolecular charge transfer (ICT) principle. The phosphate group was tethered directly to the fluorophore's phenolic OH

group, thereby preventing fluorescence in the hemicyanine core by repressing the ICT process. Upon biocatalytic dephosphorylation, free phenolic OH was regenerated, thereby reviving a strong ICT process which triggered a bright emission signal in the NIR region.

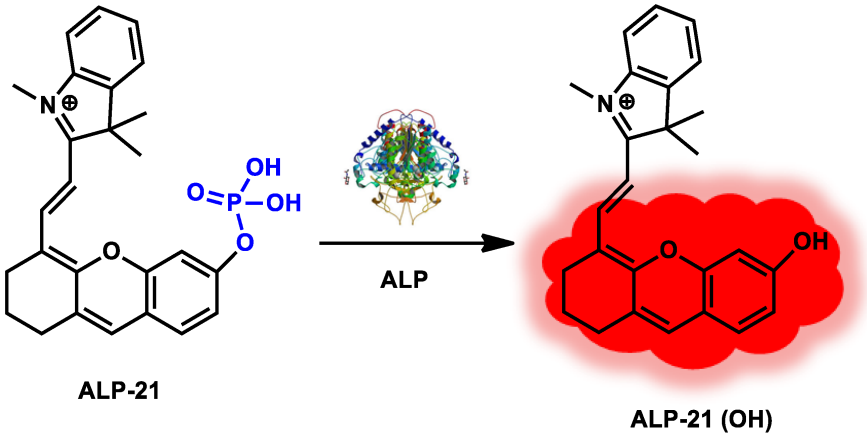

Figure 19. Structure and a plausible phosphatase recognition mechanism of the NIR fluorescent probe **ALP-21**.

Li et al. reported **ALP-22**, a water-soluble hemicyanine-based NIR fluorescent probe (**Figure 20**) tethered with a quinolinium ethyl iodide unit to induce water solubility [89]. **ALP-22** showed absorption maxima at λ_{max} 568 and 720 nm in UV–Vis spectrum, before and after addition of phosphatase, respectively. Substantial changes in absorption maxima involved a dramatic color transition from purple to blue. The phosphorylated probe was weakly emissive due to the inhibition of ICT by the phosphoester unit. Upon dephosphorylation, a strong ICT process was resurrected between the quinolinium unit and the chromene-type phenolic unit, resulting in bright emission centered at 770 nm (~7 fold). **ALP-22** showed excellent selectivity and sensitivity towards ALP in vitro, allowing it to be used to visualize ALP activity in various cells.

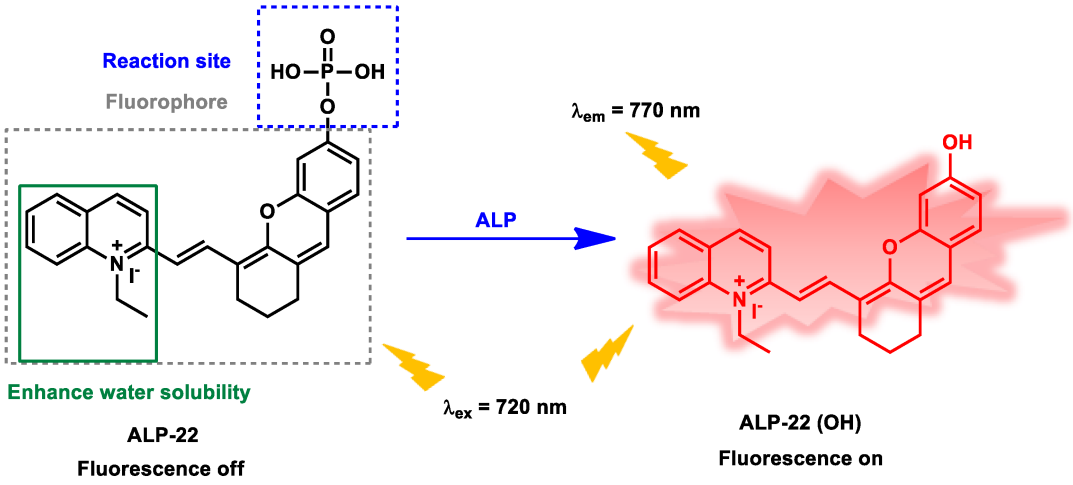

Figure 20. Structure of the quinolinium-based NIR fluorescent probe **ALP-22** and a plausible phosphatase recognition mechanism.

Zhang et al. reported a far-red fluorescent probe based on malononitrile tethered chromene analogue **ALP-23** (**Figure 21**) for in vitro and in vivo detection of ALP [90]. The design rationale of **ALP-23** was based on the phosphorylation and dephosphorylation of the phenolic OH unit, accomplished through the inhibiting and restraining of the ICT process in D–π–A confinements. The ALP-regulated dephosphorylation reaction restores the ICT effect by unveiling the “turn-on” fluorescence in the **ALP-23** (**OH**). The probe showed absorption spectra ranging from 420 to 580 nm with a sharp absorption maximum at 510 nm and annihilated red emission upon excitation at 600 nm. However, upon addition of ALP, the absorption band at 510 nm was decreased and saw a substantial shift to 605 nm. Additionally, a prominent emission signal was observed with maximal intensity at 640 nm. Such substantial changes in optical behavior in **ALP-23** were attributed to biocatalytic dephosphorylation, via the strong ICT process in **ALP-23** (**OH**).

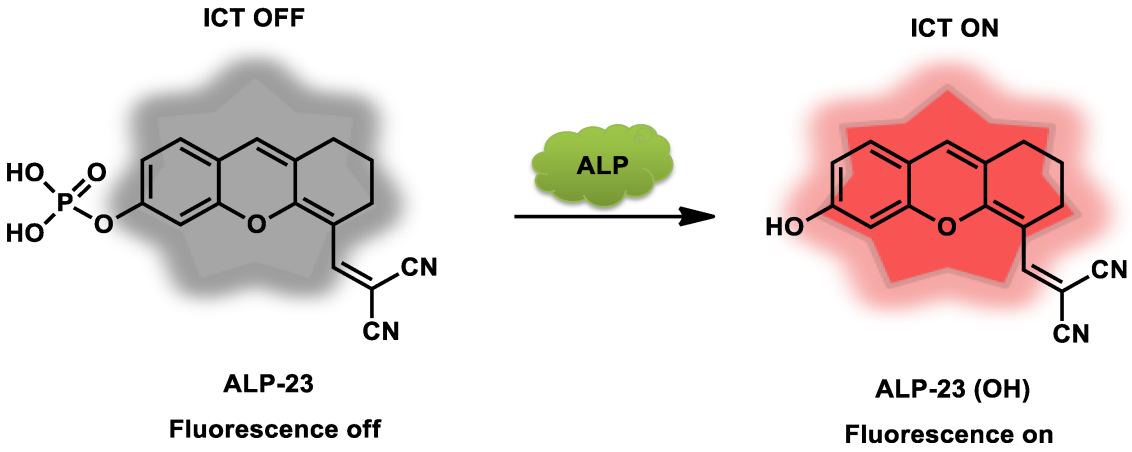

Figure 21. Structure of the di-cyanovinylene-based far-red fluorescent probe **ALP-23** and a plausible phosphatase recognition mechanism.

Khatun et al. reported coumarin-tethered triphenylphosphonium salt **ALP-24** for the recognition of (**Figure 22**) mitochondrial ALP in cellular conditions [91]. The rationale was based on a receptor-fluorophore-subcellular targeting group where coumarin acts as a signaling unit (blue fluorophore), in which the ALP receptor (diethyl phosphate) is attached to the 8th position, and the mitochondrial targeting moiety triphenylphosphine is connected to a coumarin unit through the ethyl spacer. The diethyl-phosphate moiety was retained in the molecule to enhance the cellular uptake, instead of the conventional negatively charged free phosphate terminus.

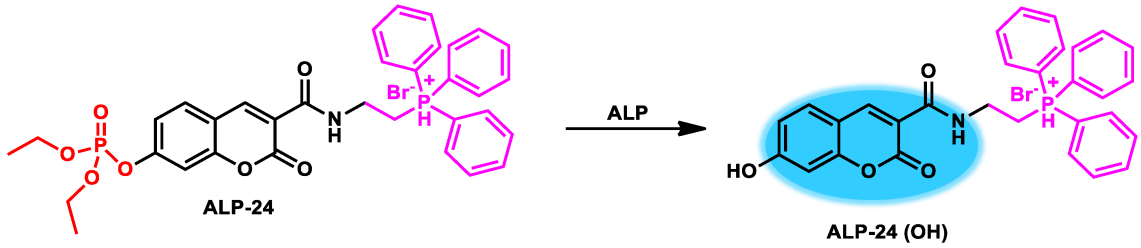

Figure 22. Structure of the mitochondria-targeting fluorescent probe **ALP-24** and a plausible phosphatase recognition mechanism.

Park et al. reported the two dihydroxanthene-based NIR fluorescent probes **ALP-25** and "**ALP-26**" (**Figure 23**) for the detection of ALP in cells and tissues [92]. To induce better water solubility, phenolic and sulfonate groups were incorporated at each terminus. The rationally designed probes were non-fluorescent in their phosphorylated states; however, upon biocatalytic dephosphorylation, the probes exhibited bright NIR fluorescence, in a dose-dependent manner. ALP-regulated *off–on* fluorescence switching in the probes was attributed to inhibition and restoration of the ICT process in the hemicyanine core. **ALP-25** and **ALP-26**, due to the minor difference in the hemicyanine core substitution, both showed a characteristic electronic absorption band around 600–700 nm in their UV–Vis absorption spectra. Both probes were weakly emissive (Φ_F = ~0.006) due to the effective inhibition of the ICT process. However, in the presence of ALP, a new band was generated at ~710 nm with a substantial increment in NIR emission intensity (~200 fold, Φ_F = ~0.009), upon excitation at 685 nm. The probes showed a rapid *switch on* response towards ALP (0.1 U min^{-1}) within 1.5 min. However, the scholars did not report any kinetic parameters, such as K_m and V_{max}, in their work.

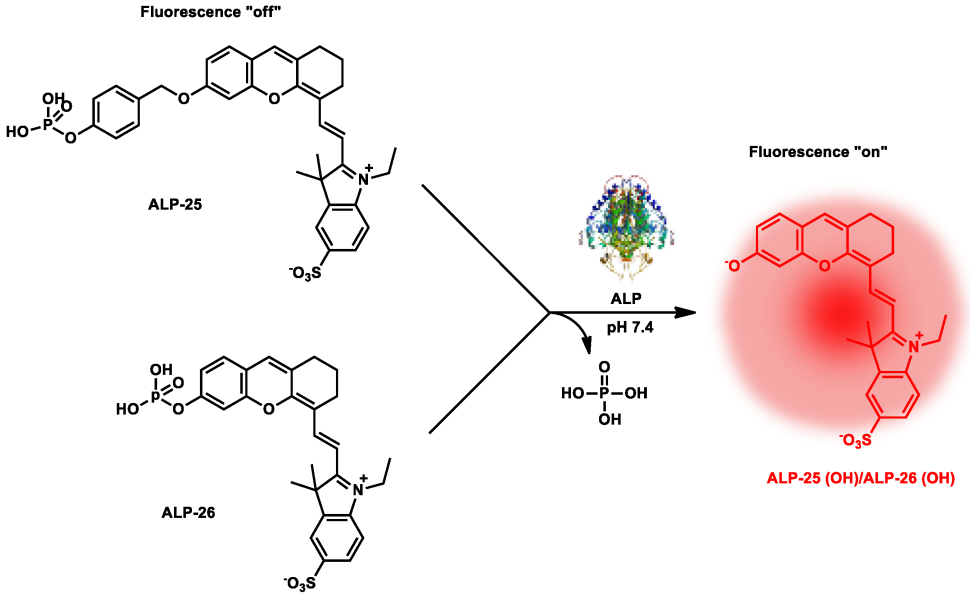

Figure 23. Structures of NIR fluorescent probes **ALP-25** and **ALP-26** and a plausible phosphatase recognition mechanism.

Upon detailed in vitro analysis, the probes' (**ALP-25** and **ALP-26**) binding affinities towards hydroxyapatite (HA) were studied in the presence of various types of calcium salts, such as phosphates, carbonates, chlorides and nitrates. Intriguingly, they showed high binding affinities towards the HA surface. The scholars believed that the phosphate unit in the probes being able to interact with the Ca^{2+} ions on the HA surface is the main reason for their superior adsorption. It was found that the probe-holding calcium phosphates scaffolds have moderately good ALP recognition capabilities in physiological conditions.

Yaqian et al. reported hydrazone-based AIE-tuned fluorescent probe €-2-(((9H-fluoren-9-ylidene) hydrazono)methyl)phenyl dihydrogen phosphate, **ALP-27**, for the recognition of cellular ALP [93]. The probe's rationale is based on the dual photophysical phenomena ESIPT and AIE. **ALP-27** exhibited a characteristic absorption maximum at 400 nm and was weakly emissive upon excitation at λ_{ex} 380 nm in physiological conditions. However, upon biocatalytic dephosphorylation, the probe showed bright emission centered at 586 nm by showing minor changes (blue shift 380 →350 nm) in the UV–Vis absorption spectra (**Figure 24**). ALP-regulated dramatic green emissive behavior exhibited a large Stokes shift (>200 nm), which was attributed to the synergistic AIE and ESIPT mechanism.

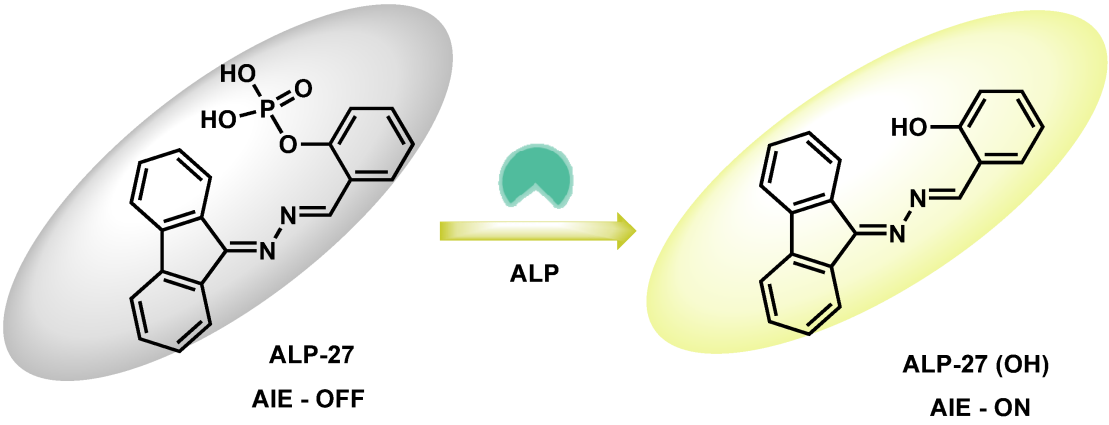

Figure 24. The structure and a plausible phosphatase recognition mechanism of the probe **ALP-27**.

Yin et al. reported a novel red emissive fluorescent probe, **ALP-28** (**Figure 25**), based on isophorone for intracellular ALP detection [94]. In physiological conditions, the probe showed an absorption maximum at 404 nm and weak emission centered at 570 nm in UV–Vis and fluorescence spectra, respectively. Upon phosphatase catalyzed hydrolysis, the probe exhibited substantial bathochromicity (404 → 421 nm) in the UV–Vis spectrum and an intense orange–yellow fluorescence signal centered at ca. 570 nm in the emission spectrum. The probe showed excellent sensitivity towards ALP with a detection limit of 0.088 U/L in in vitro assay conditions. Biocatalytic dephosphorylation of **ALP-28** was authentically validated through the ^{31}P NMR spectroscopic methods. In the studies before and after dephosphorylation, the phosphorous resonance peak was at δ −4.56 ppm or δ 0.81 ppm, respectively, unambiguously supporting the ALP-regulated phosphoester hydrolysis.

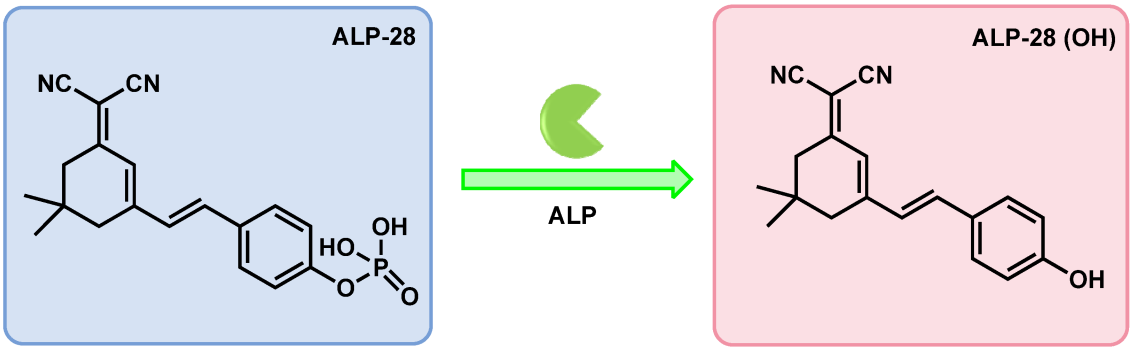

Figure 25. Structure and a plausible phosphatase recognition mechanism of the probe **ALP-28**.

Yangyang et al. reported a benzothiazole-based ratiometric probe, (4-benzamio-2-(benzo[d] thiazol-2-yl)phenyl dihydrogen phosphate (**ALP-29**), for the intracellular recognition of ALP [95]. Its molecular engineering associated it with the phosphatase-regulated ESIPT phenomenon (**Figure 26**). In order to reduce the pH-related instability in ESIPT-based probes, the phenolic's unit para position was functionalized with a benzoamide moiety. Under physiological conditions, the probe showed characteristic excitation and fluorescence emission peaks at ca. 340 and ca. 425 nm respectively. Upon biocatalytic dephosphorylation, bright red-shifted (120 nm) fluorescence emission was observed (425 nm → 545 nm). Such dramatic changes in fluorescence intensity were attributed to revival of the ESIPT mechanism, resulting from the phenolic OH unit with a benzothiazole nitrogen forming the partial quinone structure upon photochemical excitation.

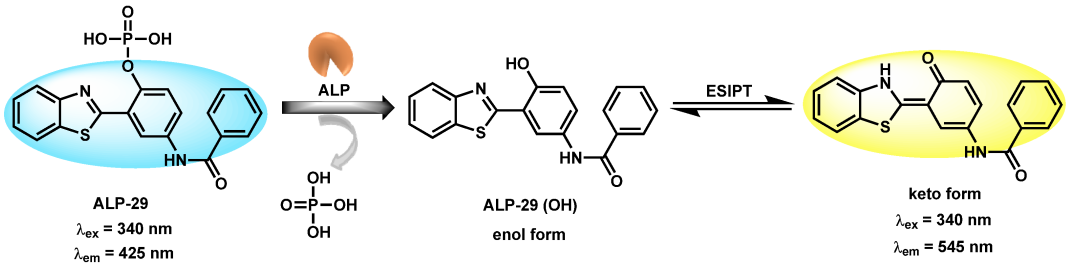

Figure 26. Structure and plausible phosphatase recognition of probe **ALP-29**.

Gao et al. reported a new blue–green emissive fluorescent probe, **ALP-30** (**Figure 27**), based on a naphthalimide core, for in cellulo ratiometric imaging of ALP [96]. In physiological conditions, **ALP-30** exhibited an absorption maximum at λ_{abs} ca. 355 nm and itself has an emission maximum at ca. 472 nm, due to the weak electron withdrawing effect (weak ICT) of its phosphoester group. Upon phosphatase assisted cleavage of the phosphoester unit, there was a new absorption maximum at λ_{abs} ca. 448 nm and a new emission peak at 556 nm, owing to the strong electron donating ability of -OH (strong ICT). Strong green emissive behavior in the dephosphorylated probe (**ALP-30** (**OH**)) can be attributed to the formation of 4-hydroxyl-naphthalimide, which resulted in the generation of the ICT process with the electron donating (resonance stabilized) phenolic OH and the electron accepting imide core.

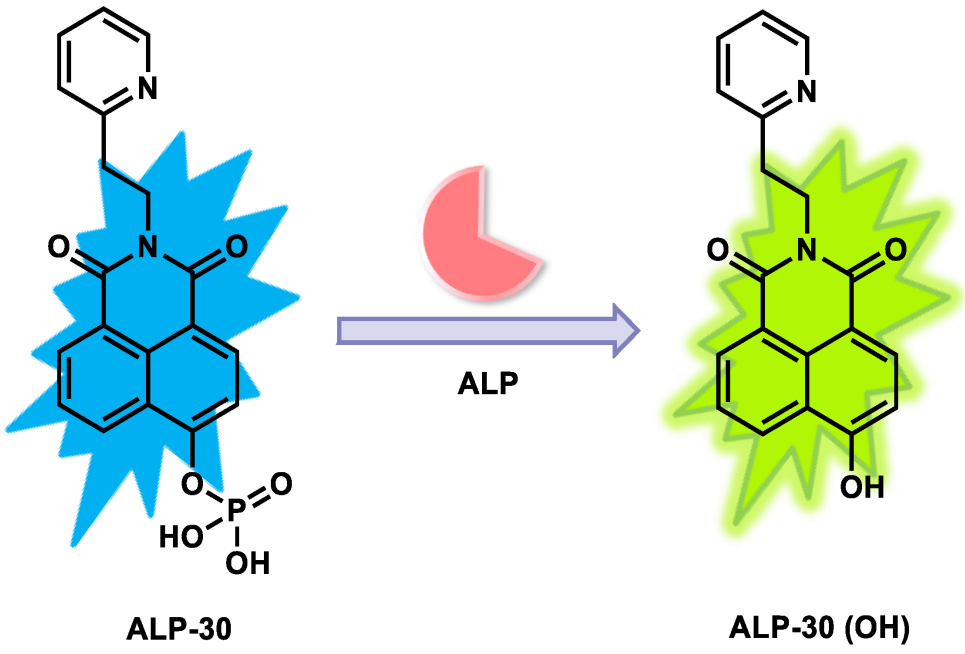

Figure 27. Structure and a plausible phosphatase recognition mechanism of **ALP-30**.

Wang et al. reported a novel hemicyanine-based water-soluble NIR fluorophore **ALP-31** (**OH**) (**Figure 28**) (3-ethyl-2-(2-(6-hydroxy-2,3-dihydro-1H-xanthen-4-yl)vinyl)benzo[d]thiazol-3-ium) for exogenous and endogenous ALP imaging in cells [97]. The probe's rationale revolved around a simple push–pull tuned ICT process between the phosphorylated/dephosphorylated phenolic OH and the benzothiazolium unit. The phosphorylated state's ICT process is inhibited due to the electron withdrawing capability of the phosphoester unit; as a result, the probe was weakly emissive (ϕ = 0.15). However, dephosphorylated **ALP-31** (**OH**) exhibited a strong fluorescence signal with an excitation maximum at ca. 680 nm and an emission maximum at ca. 723 nm. The strong ICT process between the phenolic OH and thiazolium units culminated in a Stokes' shift of 43 nm.

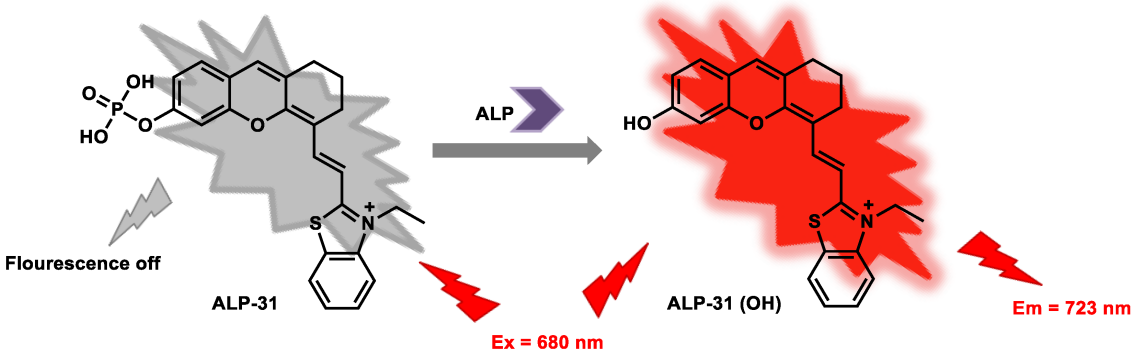

Figure 28. Structure and a plausible phosphatase recognition mechanism of **ALP-31**.

Wu et al. reported an AIE-responsive tetraphenylenthene fluorescent probe, **ALP-32** (**Figure 29**), for the recognition of ALP in living cells [98]. The probe's rationale is associated with the incorporation of a hydrophilic polar phosphate terminus —a specific receptor for ALP with a hydrophobic TPE core. In biological buffers, the probe showed a characteristic absorption maximum at λ_{max} ca. 375 nm and extremely weak emissive behavior. Upon dephosphorylation, due to the elimination and formation of polar phosphate and phenol groups, respectively, **ALP-32** (**OH**) resulted in bright green emission. These biochemically catalytic transformations led to characteristic absorption at λ_{max} ca. 400 nm and a ~12-fold enhancement in emission intensity at λ_{em} ca. 545 nm. Elevated hydrophobicity in **ALP-32** (**OH**) resulted in poor water solubility and strong green fluorescence upon aggregation through the AIE mechanism.

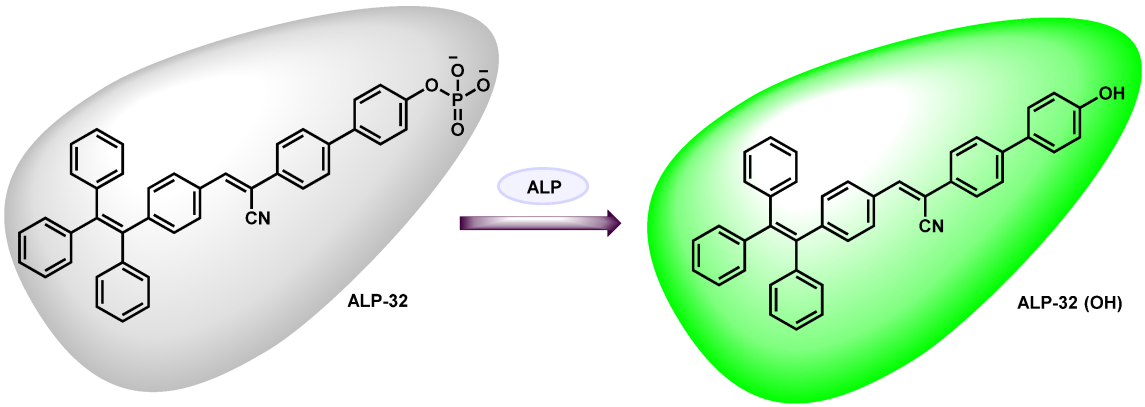

Figure 29. Structure and a plausible phosphatase recognition mechanism of probe **ALP-32**.

Table 1. List of the small phosphorylated molecular probes for ALP activity in cells/tissues/in vivo models.

Probes	Linear Range	k_{cat}/K_M Value	Detection Limit	Response Time	Stokes Shift	$\lambda_{ex}/\lambda_{em}$ (nm)	Quantum Yield (Φ)	IC_{50} Value	Sensing Mode	Application	Cytotoxicity	L
ALP-1, ALP-2, ALP-3	10–50 mU/mL, 10–40 mU/mL	/	/	/	/	338/469, 337/457, 337/469	0.075, 0.118, 0.101	/	Turn-on Fluorescence	Cellular imaging in living stem cells	30 μM	B m
ALP-4	0–150 U/L	/	0.15 U/L	/	211 nm	430/539, 641	/	/	Ratiometric	Live cell imaging	20 μM	I
ALP-5	0.5–10 U/L	/	0.30 U/L	/	135 nm	365/500	/	7.39 μM	Turn-on Fluorescence	In living cells and tissues	20 μM	C

ALP-6	0.01–2.0 U/mL	/	0.003 U/mL	20 min	/	690/738	/	141.9 μM	Turn-on Near-Infrared Fluorescence	In Vivo Cell, tissue and living animal	30.0 μM	
ALP-7	0–2.8 U/mL	/	0.06 U/mL	2 h	/	465/530	/	/	Turn-Off Fluorescence	in Vitro and in Living Cells	160 μM	
ALP-8	0–0.1 U/mL	1.01×10^5 M^{-1} s^{-1}	0.07 U/L	2 min	/	680/700	/	7.51 μM	Off–On Near-infrared Fluorescence	Living Cells and Mice	20 μM	
ALP-9	0.5–8.0 U/L	/	0.072 U/L	/	/	535/683	/	/	Rational Turn-on Red-Near-Infrared fluorescence	In vivo and in vitro	50 μM	M
ALP-10	0–60 mU/mL	/	0.072 mU/mL	/	260 nm	390/476, 650	0.16	10 μM	Ratiometric	living cells and in vivo	10 μM	M
ALP-11, ALP-12	/	/	/	/	/	405/500–530	/	10 μM	Turn-on Fluorescence	Living cells and zebrafish model	10 μM	
ALP-13	/	1.4×10^4 M^{-1} s^{-1}	/	/	/	472/542	0.002	36 μM	Turn-on Fluorescence	Living cells	10 μM	
ALP-14	/	1.7×10^4 M^{-1} s^{-1}	1.09 U/L	/	/	550/585	0.0023	7.58 μM	Turn-on Fluorescence	Living cells	/	
ALP-15	0–10 U/L	/	0.012 U/L	/	180 nm	356/536	/	/	Turn-on Fluorescence	Living cells	/	
ALP-16	/	/	0.38 U/L	/	/	425/554	/	/	Ratiometric	In vivo	5 μM	
ALP-17	20–180 U/L	/	2.3 U/L	/	/	405/410–460, 470–530	0.41	/	Ratiometric	Living cells	20 μM	
ALP-18	/	13.6×10^5 M^{-1} s^{-1}	0.011 U/L	/	/	490/540	0.0487	/	Turn-on Fluorescence	In vitro, cell imaging and cell cultures	100.0 μM	
ALP-19	50–200 U/L	/	3.8 U/L	30 min	/	440/550	0.105	/	Ratiometric	Living cells	10 μM	
ALP-20	/	/	0.032 U/L	/	/	400–410/455	0.085	/	Turn-on Fluorescence	Live cells and serum samples	50 μM	
ALP-21	1–30 U/L	/	0.28 U/L	/	/	680/690–800	/	/	Turn-on Fluorescence	In vivo and in vitro	20 μM	
ALP-22	0.05–1.0 U mL^{-1}	/	0.017 U mL^{-1}	/	/	720/770	/	109.6 μM	Turn-on Fluorescence	Cell imaging, treatment of diabetes	30 μM	
ALP-23	5–100 U/L	/	0.28 U/L	/	/	600/620–850	/	141.4 μM	Turn-on Fluorescence	Living cells and zebrafish	10 μM	
ALP-24	/	3.12×10^6 M^{-1} s^{-1}	2.921 ng/mL	/	/	410/450	0.567	/	Ratiometric	Live cells	50 μM	M

ALP-25, ALP-26	0–1.0 U mL^{-1}	/	10^{-5}–10^{-3} U mL^{-1}	1.5 min	/	685/710	0.13	/	Turn-on fluorescence	In vivo	50 μM	
ALP-27	1–100 U/L	/	0.6 U/L	/	>200 nm	380/586	/	/	Turn-on fluorescence	Living cells	10 μM	Li
ALP-28	/	/	0.088 U/L	6 min	/	440/570	/	/	Turn-on Fluorescence	Living cells	10 μM	
ALP-29	/	/	0.004 mU/mL	35 min	/	340/545	0.028	/	Ratiometric	Living cells	20 μM	
ALP-30	0–200 U/L	/	0.25 U/L	/	/	425/472	/	/	Ratiometric	Living cells	/	
ALP-31	0–8 U/L	/	0.042 U/L	/	43 nm	680/723	0.15	23.98 μM	Turn-on Near-Infrared Fluorescence	Living cells	20 μM	
ALP-32	/	/	14.2 U/L	/	/	440/543	/	/	Turn-on Fluorescence	Live cells	50 μM	
ALP-33	0.05–1.05 U/mL	/	0.012 U/mL	/	/	377/572	0.0392	/	Colorimetric and fluorescent on-off-on	Over expressed cancer cells & normal salivary gland cells	25 μM	
ALP-34	/	/	/	/	/	/	/	/	Turn-on fluorescence (NIR fluorescence)	In vitro and live cells	/	
ALP-35	0.01–2.5 U/mL	/	0.0033 U/mL	/	/	685/718	/	148.6 μM	Turn-on fluorescence (NIR fluorescence)	In vivo	/	

4. Organo-Metallic-Based Fluorescent Probes

Seo et al. reported the fluorescein/hydrazine-based probe **ALP-33** (**Figure 30**) to investigate ALP activity in cellular systems by measuring the consumption of trace amounts of PPi in the intracellular matrix [99]. With this indirect strategy, the green emissive probe **ALP-33** was designed to detect Cu^{2+}/Ppi under physiological conditions in a sequential manner. In this sequential analysis, *on–off–on* switching properties were observed upon sequential addition of Cu^{2+} and PPi ions. In addition, dramatic color transitions occurred from colorless → yellow → colorless. **ALP-33** showed a characteristic absorption maximum at 370 nm in the UV–Vis absorption spectrum. However, upon addition of Cu^{2+} ions, a new band at 446 nm was generated, making the solution an intense yellow color.

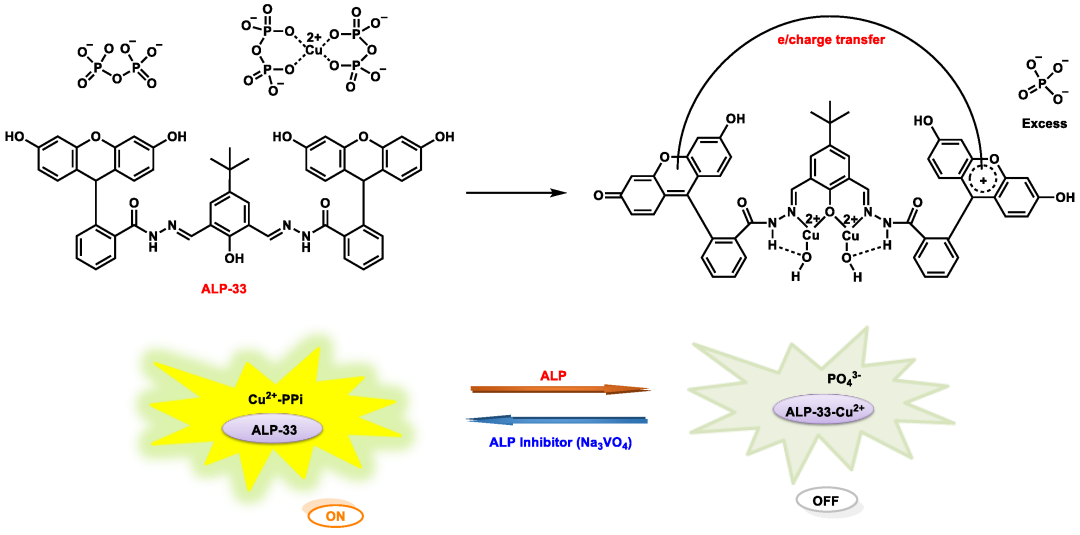

Figure 30. Plausible recognition mechanism of Cu^{2+}/Ppi and intracellular ALP activity using **ALP-33**.

In a detailed investigation, endogenous ALP activity was monitored in normal salivary gland cells and cancer cell lines. By tracking the intracellular PPi, by employing a Cu^{2+} entity, the alkaline phosphatase activity was monitored in the presence of a fixed dose of an inhibitor (Na_3VO_4) in ALP-overexpressing cancer cells and normal salivary gland cell lines. In the time and dose-dependent study, the scholars used specified amounts of **ALP-33**–Cu^{2+} complex for specified numbers of

cells. Upon detailed analysis of PPi amounts produced in cancer cells at specified conditions, endogenous ALP activity was monitored at different time intervals. Intriguingly, complex-incubated cells (cancer and normal cells) showed bright green emission only in the presence of Na_3VO_4 (inhibitor). Relative signal intensities in cancer cells were higher than in normal cells due to rapid mitotic divisions, which resulted in the generation of large amounts of PPi in cells.

5. Nanomaterial-Based Fluorescent Probes

Lim et al. developed a new type of nanocomposite by formulating the doping of FDA-approved indocyanine green (IcyG), a fluorescent material, onto hydroxyapatite, followed by its surface modification through gold nanoparticles. This composite, **ALP-34** [100], was made for the recognition of ALP activity during the osteoblast differentiation process (**Figure 31**).

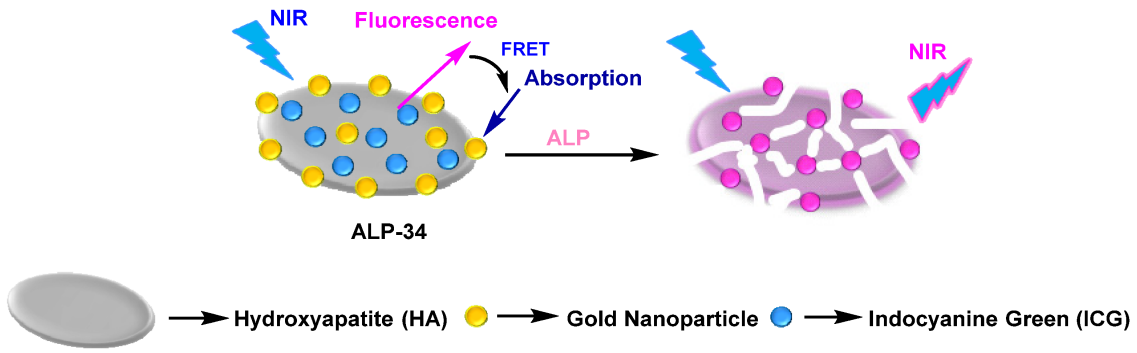

Figure 31. Schematic representation of gold nanoparticles conjugated with fluorescent hydroxyapatite (**ALP-34**) for the detection of alkaline phosphatase activity.

Compared to organometallic complexes, nanomaterials are more promising candidates for the in vitro and in vivo recognition of ALP activity. This is because nano-sized functional materials usually show excellent cell transfusion capabilities, along with excellent photo-stability. Depending on surface functionalization, nanomaterials cellular localizations can be regulated. Even though not many fluorescent nano-materials have been reported for the in vitro, in cellulo recognition of phosphatase, and for their applications in cancer related systems, in near future, next generation nanomaterials could emerge as promising candidates for phosphatase-associated diagnostic tools for cancer and diagnostic tools for other diseases.

6. Miscellaneous

Ou-Yang et al. reported an NIR-based infinite coordination polymer nanoparticle (**ALP-35**) (**Figure 32**) for endogenous ALP activity detection in in cellulo and in vivo models[101]. The rationally designed nanoprobe was constructed based on doping of fluorescent dye into a metal-ion-driven co-ordinational supramolecular nano-assembly. Accordingly, NIR emissive hemicyanine dyes were doped into Tb^{3+}-GMP, an infinite nano-co-ordinational polymer. Due to the proximity induced quenching in confined spaces in the metal nano-coordination polymer, NIR emissive behavior was diminished. However, upon dephosphorylation, self-assembled metal nanostructures gradually dissolved by releasing NIR dye. The nanoprobe showed a sharp absorption band at ca. 695 nm and weak emission centered at 738 nm upon excitation at 685 nm. Paradoxically, upon ALP-catalyzed dephosphorylation of GMP, there was bright NIR emission centered at 738 nm (~8-fold) and substantial hyperchromicity in the absorption spectrum.

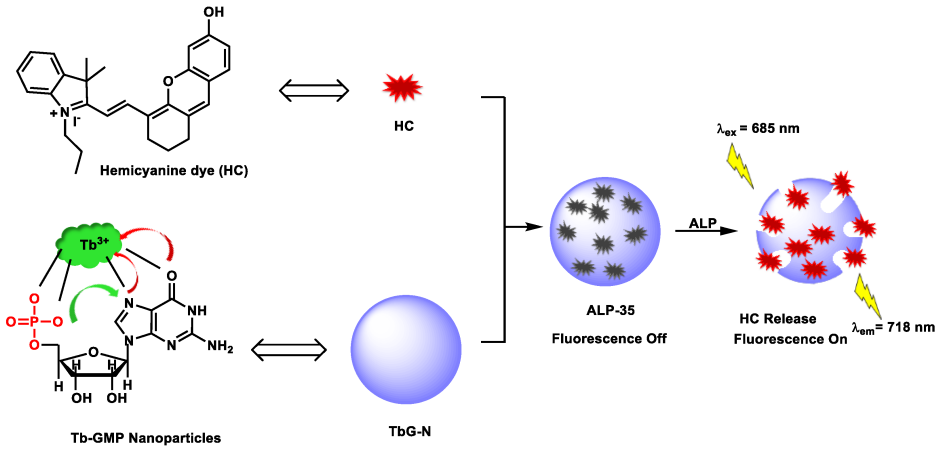

Figure 32. Schematic representation of the **ALP-35** nanoprobe's design and a plausible phosphatase recognition mechanism.

ALP-35 showed a good catalytic constant (k_{cat} ~ 0.03 s^{-1}) and the detection limit of 0.0033 U/mL towards phosphatase, and showed no interference from biologically relevant molecules, such as GOX, EXO and trypsin. Inhibitor assay studies with sodium orthovanadate (Na_3VO_4) showed an IC_{50} of 148.6 μM for ALP in similar experimental conditions.

References

1. Liang, J.; Kwok, R.T.K.; Shi, H.; Tang, B.Z.; Liu, B. Fluorescent Light-up Probe with Aggregation-Induced Emission Cha racteristics for Alkaline Phosphatase Sensing and Activity Study. ACS Appl. Mater. Interfaces 2013, 5, 8784–8789.
2. McComb, R.B.; Bowers, G.N., Jr.; Posen, S. Alkaline Phosphatase, 1st ed.; Springer: New York, NY, USA; Plenum Pres s: New York, NY, USA, 1979.
3. Yu, L.; Feng, L.; Xiong, L.; Li, S.; Xu, Q.; Pan, X.; Xiao, Y. Rational design of dual-emission lanthanide metal-organic fra mework for visual alkaline phosphatase activity assay. ACS Appl. Mater. Interfaces 2021, 13, 11646–11656.
4. Ma, F.; Liu, M.; Zhang, C.-Y. Ligase amplification reaction-catalyzed assembly of a single quantum dot-based nanosens or for sensitive detection of alkaline phosphatase. Chem. Commun. 2019, 55, 8963–8966.
5. Haarhaus, M.; Brandenburg, V.; Kalantar-Zadeh, K.; Stenvinkel, P.; Magnusson, P. Alkaline phosphatase: A novel treat ment target for cardiovascular disease in CKD. Nat. Rev. Nephrol. 2017, 13, 429–442.
6. Zhang, W.; Gao, Y.; Li, Y.; Zhang, Q.; Hu, Z.; Zhang, Y.; Hussain, E.; Yang, X.; Yu, D.; Yu, C. Polyphosphoric acid-induc ed perylene probe self-assembly and label-free fluorescence turn-on detection of alkaline phosphatase. Anal. Bioanal. Chem. 2017, 409, 1031–1036.
7. Yang, D.; Guo, Z.; Tang, Y.; Miao, P. Poly(thymine)-templated selective formation of copper nanoparticles for alkaline p hosphatase analysis aided by alkyne-azide cycloaddition “Click” reaction. ACS Appl. Nano Mater. 2018, 1, 168–174.
8. Liu, X.-G.; Xing, X.-J.; Li, B.; Guo, Y.-M.; Zhang, Y.-Z.; Yang, Y.; Zhang, L.-F. Fluorescent assay for alkaline phosphatas e activity based on graphene oxide integrating with λ exonuclease. Biosens. Bioelectron. 2016, 81, 460–464.
9. Hu, X.-L.; Wu, X.-M.; Fang, X.; Li, Z.-J.; Wang, G.-L. Switchable fluorescence of gold nanoclusters for probing the activi ty of alkaline phosphatase and its application immunoassay. Biosens. Bioelectron. 2016, 77, 666–672.
10. Liu, S.; Pang, S.; Na, W.; Su, X. Near-infrared fluorescence probe for the determination of alkaline phosphatase. Biose ns. Bioelectron. 2014, 55, 249–254.
11. Halawa, M.I.; Gao, W.; Saqib, M.; Kitte, S.A.; Wu, F.; Xu, G. Sensitive detection of alkaline phosphatase by switching o n gold nanoclusters fluorescence quenched by pyridoxal phosphate. Biosens. Bioelectron. 2017, 95, 8–14.
12. Rao, G.M.M.; Morghom, L.O. Correlation between serum alkaline phosphatase activity and blood glucose levels. Enzy me 1986, 35, 57–59.
13. Sharma, U.; Pal, D.; Prasad, R. Alkaline Phosphatase: An Overview. Ind. J. Clin. Biochem. 2014, 29, 269–278.
14. Wang, X.; Zhang, Z.; Ma, X.; Wen, J.; Geng, Z.; Wang, Z. Real-time fluorescence assays of alkaline phosphatase and ATP sulfurylase activities based on a novel PPi fluorescent probe. Talanta 2015, 137, 156–160.
15. Deng, J.; Yu, P.; Wang, Y.; Mao, L. Real-time ratiometric fluorescent assay for alkaline phosphatase activity with stimulu s responsive infinite coordination polymer nanoparticles. Anal. Chem. 2015, 87, 3080–3086.
16. Zheng, F.; Guo, S.; Zeng, F.; Li, J.; Wu, S. Ratiometric fluorescent probe for alkaline phosphatase based on betaine-mo dified polyethylenimine via excimer/monomer conversion. Anal. Chem. 2014, 86, 9873–9879.
17. Zhang, L.; Zhao, J.; Duan, M.; Zhang, H.; Jiang, J.; Yu, R. Inhibition of dsDNA-templated copper nanoparticles by pyrop hosphate as a label-free fluorescent strategy for alkaline phosphatase assay. Anal. Chem. 2013, 85, 3797–3801.
18. Wang, H.B.; Li, Y.; Chen, Y.; Zhang, Z.P.; Gan, T.; Liu, Y.M. Determination of the activity of alkaline phosphatase by usin g nanoclusters composed of flowerlike cobalt oxyhydroxide and copper nanoclusters as fluorescent probes. Microchim. Acta 2018, 185, 102.
19. Li, G.; Huili Fu, H.; Chen, X.; Gong, P.; Chen, G.; Xia, L.; Wang, H.; You, J.; Wu, Y. Facile and sensitive fluorescence se nsing of alkaline phosphatase activity with photoluminescent carbon dots based on inner filter effect. Anal. Chem. 2016, 88, 2720–2726.
20. Cox, W.G.; Singer, V.L. A High-resolution, fluorescence-based method for localization, of endogenous alkaline phospha tase activity. J. Histochem. Cytochem. 1999, 47, 1443–1455.
21. Butterworth, P.J. Biochemistry of alkaline phosphatases. Cell Biochem. Funct. Biochem. Data 1983, 1, 66–69.
22. Štefková, K.; Procházková, J.; Pacherník, J. Alkaline phosphatase in stem cells. Stem Cells Int. 2015, 2015, 628368.
23. Millan, J.L. Alkaline Phosphatases Structure, substrate specificity and functional relatedness to other members of a larg e superfamily of enzymes. Purinergic Signal. 2006, 2, 335–341.
24. Chen, S.L.; Liao, R.Z. Phosphate monoester hydrolysis by trinuclear alkaline phosphatase; DFT study of transition stat es and reaction mechanism. ChemPhysChem 2014, 15, 2321–2330.
25. Holtz, K.M.; Kantrowitz, E.R. The mechanism of the alkaline phosphatase reaction: Insights from NMR, crystallography and site-specific mutagenesis. FEBS Lett. 1999, 462, 7–11.

26. Holtz, K.M.; Stec, B.; Kantrowitz, E.R. A model of the transition state in the alkaline phosphatase reaction. J. Biol. Che m. 1999, 274, 8351–8354.

27. Chaudhuri, G.; Selvaraj, U.; Babu, V.; Thilagaraj, R.W.. Recent Trends in Phosphatase-Mediated Bioremediation; In Ph osphoric Acid Industry Problems and Solutions; IntechOpen: London, UK, 2017; pp. 27–46.

28. W Meyer-Sabellek; P Sinha; E Köttgen; Alkaline phosphatase. Laboratory and clinical implications.. *Journal of chromat ography* **1988**, *429*, 419-44, .

29. Krupaa, R.J.; Hariharan, R.; Babu, N.A.; Masthan, K.M.K. Alkaline phosphatase and its clinical importance-A review. Eu r. J. Mol. Clin. Med. 2020, 7, 1409–1413.

30. Thanih Balbaied, T.; Moore, E. Overview of optical and electrochemical alkaline phosphatase (ALP) biosensors: Recent approaches in cells culture techniques. Biosensors 2019, 9, 102.

31. Nsabimana, A.; Lan, Y.; Du, F.; Wang, C.; Zhang, W.; Xu, G. Alkaline phosphatase-based electrochemical sensors for h ealth applications. Anal. Methods 2019, 11, 1996–2006.

32. Goggins, S.; Naz, C.; Marsh, B.J.; Frost, C.G. Ratiometric electrochemical detection of alkaline phosphatase. Chem. C ommun. 2015, 51, 561–564.

33. Miao, P.; Ning, L.; Li, X.; Shu, Y.; Li, G. An electrochemical alkaline phosphatase biosensor fabricated with two DNA pro bes coupled with lambda exonuclease. Biosens. Bioelectron. 2011, 27, 178–182.

34. Kim, H.-U.; Kim, H.Y.; Kulkarni, A.; Ahn, C.; Jin, Y.; Kim, Y.; Lee, K.-N.; Lee, M.-H.; Kim, T. A sensitive electrochemical s ensor for in vitro detection of parathyroid hormone based on a MoS2-graphene composite. Sci. Rep. 2016, 6, 34587.

35. Sun, D.; Xu, W.; Liang, C.; Shi, W.; Xu, S. Smart surface-enhanced resonance Raman scattering nanoprobe for monito ring cellular alkaline phosphatase activity during osteogenic differentiation. ACS Sens. 2020, 5, 1758–1767.

36. Dai, X.; Lu, L.; Zhang, X.; Song, Z.-L.; Song, W.; Chao, Q.; Li, Q.; Wang, W.; Chen, J.; Fan, G.C.; et al. MnO2 shell-isol ated SERS nanoprobe for the quantitative detection of ALP activity in trace serum: Relying on the enzyme-triggered etc hing of MnO2 shell to regulate the signal. Sens. Actuators B Chem. 2021, 334, 129605.

37. Yi-Wei, T.; Charles, W.S. Advanced Techniques in Diagnostic Microbiology, 2nd ed.; Springer: New York, NY, USA, 201 3.

38. Roelofs, H.; Manes, T.; Janszen, T.; Millan, J.L.; Oosterhuis, J.W.; Looijenga, L.H.J. Heterogeneity in alkaline phosphat ase isozyme expression in human testicular germ cell tumours: An enzyme-/immunohistochemical and molecular analy sis. J. Pathol. 1999, 189, 236–244.

39. Mano, H.; Furuhashi, Y.; Morikawa, Y.; Hattori, S.E.; Goto, S.; Tomoda, Y. Radioimmunoassay of placental alkaline-pho sphatase in ovarian-cancer sera and tissues. Obstet. Gynecol. 1986, 68, 759–764.

40. Degroote, G.; Dewaele, P.; Vandevoorde, A.; Debroe, M.; Fiers, W. Use of monoclonal-antibodies to detect human plac ental alkaline-phosphatase. Clin. Chem. 1983, 29, 115–119.

41. Sekar, S.; Giermanska, J.; Chapel, J.P. Reusable and recyclable quartz crystal microbalance sensors. Sens. Actuators B Chem. 2015, 212, 196–199.

42. Kacar, T.; Zin, M.T.; So, C.; Wilson, B.; Ma, H.; Gul-Karaguler, N.; Tamerler, C. Directed self-immobilization of alkaline p hosphatase on micro-patterned substrates via genetically fused metal-binding peptide. Biotechnol. Bioeng. 2009, 103, 696–705.

43. Jang, H.J.; Ahn, J.; Kim, M.G.; Shin, Y.B.; Jeun, M.; Cho, W.J.; Lee, K.H. Electrical signaling of enzyme-linked immunos orbent assays with an ion-sensitive field-effect transistor. Biosens. Bioelectron. 2015, 64, 318–323.

44. Li, C.M.; Zhen, S.J.; Wang, J.; Li, Y.F.; Huang, C.Z. A gold nanoparticles-based colorimetric assay for alkaline phosphat ase detection with tunable dynamic range. Biosens. Bioelectron. 2013, 43, 366–371.

45. Hu, Q.; He, M.; Mei, Y.; Feng, W.; Jing, S.; Kong, J.; Zhang, X. Sensitive and selective colorimetric assay of alkaline ph osphatase activity with Cu(II)-phenanthroline complex. Talanta 2017, 163, 146–152.

46. Hu, X.; Sun, C.; Shi, Y.; Long, Y.; Zheng, H. Colorimetric sensing of alkaline phosphatase and a-fetoprotein based on th e photoinduced oxidase activity of fluorescein. New J. Chem. 2019, 43, 4525–4530.

47. Upadhyay, Y.; Kumar, R.; Sahoo, S.K. Developing a cost-effective bioassay to detect alkaline phosphatase activity and generating white light emission from a single nano-assembly by conjugating Vitamin B6 cofactors with lysozyme-stabili zed fluorescent gold nanoclusters. ACS Sustain. Chem. Eng. 2020, 8, 4107–4113.

48. Westmeyer, G.G.; Emer, Y.; Lintelmann, J.; Jasanoff, A. MRI-based detection of alkaline phosphatase gene reporter act ivity using a porphyrin solubility switch. Chem. Biol. 2014, 21, 422–429.

49. Zhang, Q.; Li, S.; Fu, C.; Xiao, Y.; Zhang, P.; Ding, C. Near-infrared mito-specific fluorescent probe for ratiometric detec tion and imaging of alkaline phosphatase activity with high sensitivity. J. Mater. Chem. B 2019, 7, 443–445.

50. Pandith, A.; Seo, Y.J. Label-free sensing platform for miRNA-146a based on chromo-fluorogenic pyrophosphate recogn ition. J. Inorg. Biochem. 2020, 203, 110867.

51. Pandith, A.; Koo, J.; Seo, Y.J. Daphnetin: A novel blue-green photonic switch for disodium phosphates that allows monit oring of polymerase chain reactions. Spectrochim. Acta Part A 2018, 204, 620–628.

52. Pandith, A.; Siddappa, R.G.; Seo, Y.J. Recent developments in novel blue/green/red/NIR small fluorescent probes for in cellulo tracking of RNA/DNA G-quadruplexes. J. Photochem. Photobiol. C Rev. 2019, 40, 81–116.

53. Zhang, H.; Ju, Q.; Pang, S.; Wei, N.; Zhang, Y. Recent progress of fluorescent probes for the detection of alkaline phos phatase (ALP): A review. Dyes Pigments 2021, 194, 109569.

54. Wang, K.; Wang, W.; Zhang, X.Y.; Jiang, A.Q.; Yang, Y.S.; Zhu, H.L. Fluorescent probes for the detection of alkaline ph osphatase in biological systems: Recent advances and future prospects. Trends Anal. Chem. 2021, 136, 116189.

55. Gwynne, L.; Sedgwick, A.C.; Gardiner, J.E.; Williams, G.T.; Kim, G.; Lowe, J.P.; Maillard, J.Y.; Jenkins, A.T.A.; Bull, S. D.; Sessler, J.L.; et al. Long wavelength TCF-based fluorescent probe for the detection of alkaline phosphatase in live c ells. Front. Chem. 2019, 7, 255.

56. Jidong, Z.; Hongze, L.; Li, M. Research Progress in the Fluorescent Probes for Alkaline Phosphatase. Chin. J. Org. Ch em. 2019, 39, 3132–3144.

57. Li, M.; Gurram, B.; Lei, S.; Blum, N.T.; Huang, P.; Lin, J. Recent advances in fluorescence imaging of alkaline phosphat ase. Chin. Chem. Lett. 2021, 32, 1316–1330.

58. Liu, H.W.; Chen, L.; Xu, C.; Li, Z.; Zhang, H.; Zhang, X.B.; Tan, W. Recent progresses in small-molecule enzymatic fluo rescent probes for cancer imaging. Chem. Soc. Rev. 2018, 47, 7140–7180.

59. Niu, X.; Ye, K.; Wang, L.; Lin, Y.; Du, D. A review on emerging principles and strategies for colorimetric and fluorescent detection of alkaline phosphatase activity. Anal. Chim. Acta 2019, 1086, 29–45.

60. Han, Y.; Chen, J.; Li, Z.; Chen, H.; Qiu, H. Recent progress and prospects of alkaline phosphatase biosensor based on fluorescence strategy. Biosens. Bioelectron. 2020, 148, 111811.

61. Hu, L.; Zhang, Q.; Gan, X.; Yin, W.; Fu, W. Switchable fluorescence of MoS2 quantum dots: A multifunctional probe for sensing of chromium (VI), ascorbic acid, and alkaline phosphatase activity. Anal. Bioanal. Chem. 2018, 410, 7551–755 7.

62. Syahir, A.; Usui, K.; Tomizaki, K.Y.; Kajikawa, K.; Mihara, H. Label and label-free detection techniques for protein micro arrays. Microarrays 2015, 4, 228–244.

63. Boaro, A.; Ageitos, L.; Torres, M.; Bartoloni, F.H.; de la Fuente-Nunez, C. Light-emitting probes for labeling peptides. Ce ll Rep. Phys. Sci. 2020, 1, 100257.

64. Upadhyay, Y.; Kumar, R.; Sk, A.K.; Sahoo, S.K. Vitamin B6 cofactors conjugated ovalbumin-stabilized gold nanocluster s: Application in alkaline phosphatase activity detection and generating white-light emission. Microchem. J. 2020, 156, 104859.

65. Upadhyay, Y.; Bothra, S.; Kumar, R.; Sk, A.K.; Sahoo, S.K. Mimicking biological process to detect alkaline phosphatase activity using the vitamin B6 cofactor conjugated bovine serum albumin capped CdS quantum dots. Colloids Surf. B Bio interfaces 2020, 185, 110624.

66. Wang, J.H.; Wang, K.; Bartling, B.; Liu, C.C. The detection of alkaline phosphatase using an electrochemical biosensor in a single-step approach. Sensors 2009, 9, 8709–8721.

67. Li, X.; Wang, X.; Guo, W.; Wang, Y.; Hua, Q.; Tang, F.; Luan, F.; Tian, C.; Zhuang, X.; Zhao, L. Selective Detection of Al kaline Phosphatase Activity in Environmental Water Samples by Copper Nanoclusters Doped Lanthanide Coordination Polymer Nanocomposites as the Ratiometric Fluorescent Probe. Biosensors 2022, 12, 372.

68. Cao, Y.; Yu, X.; Sun, C.; Cui, J. Theoretical Investigation on the ESIPT Process and Detection Mechanism for Dual-Prot on Type Fluorescent Probe. Int. J. Mol. Sci. 2022, 23, 2132.

69. Sun, T.; Xia, N.; Liu, L. A graphene oxide-based fluorescent platform for probing of phosphatase activity. Nanomaterials 2016, 6, 20.

70. David, C.I.; Prabakaran, G.; Nandhakumar, R. Recent approaches of 2HN derived fluorophores on recognition of Al3+ i ons: A review for future outlook. Microchem. J. 2021, 169, 106590.

71. Cao, F.Y.; Long, Y.; Wang, S.B.; Li, B.; Fan, J.X.; Zeng, X.; Zhang, X.Z. Fluorescence light-up AIE probe for monitoring cellular alkaline phosphatase activity and detecting osteogenic differentiation. J. Mater. Chem. B 2016, 4, 4534–4541.

72. Song, Z.; Kwok, R.T.; Zhao, E.; He, Z.; Hong, Y.; Lam, J.W.; Liu, B.; Tang, B.Z. A ratiometric fluorescent probe based on ESIPT and AIE processes for alkaline phosphatase activity assay and visualization in living cells. ACS Appl. Mater. Inte rfaces 2014, 6, 17245–17254.

73. Zhang, H.; Xiao, P.; Wong, Y.T.; Shen, W.; Chhabra, M.; Peltier, R.; Jiang, Y.; He, Y.; He, J.; Tan, Y.; et al. Construction of an alkaline phosphatase-specific two-photon probe and its imaging application in living cells and tissues. Biomaterial s 2017, 140, 220–229.

74. Li, S.J.; Li, C.Y.; Li, Y.F.; Fei, J.; Wu, P.; Yang, B.; Ou-Yang, J.; Nie, S.X. Facile and sensitive near-infrared fluorescence probe for the detection of endogenous alkaline phosphatase activity in vivo. Anal. Chem. 2017, 89, 6854–6860.

75. Dong, L.; Miao, Q.; Hai, Z.; Yuan, Y.; Liang, G. Enzymatic hydrogelation-induced fluorescence turn-off for sensing alkali ne phosphatase in vitro and in living cells. Anal. Chem. 2015, 87, 6475–6478.

76. Tan, Y.; Zhang, L.; Man, K.H.; Peltier, R.; Chen, G.; Zhang, H.; Zhou, L.; Wang, F.; Ho, D.; Yao, S.Q.; et al. Reaction-ba sed off–on near-infrared fluorescent probe for imaging alkaline phosphatase activity in living cells and mice. ACS Appl.

Mater. Interfaces 2017, 9, 6796–6803.

77. Jie, X.; Wu, M.; Yang, H.; Wei, W. Red–Near-Infrared Fluorescent Probe for Time-Resolved in Vivo Alkaline Phosphata se Detection with the Assistance of a Photoresponsive Nanocontainer. Anal. Chem. 2019, 91, 13174–13182.

78. Zhang, P.; Fu, C.; Zhang, Q.; Li, S.; Ding, C. Ratiometric fluorescent strategy for localizing alkaline phosphatase activity in mitochondria based on the ESIPT process. Anal. Chem. 2019, 91, 12377–12383.

79. Jia, Y.; Li, P.; Han, K. AMP/GMP analogs as affinity ESIPT probes for highly selective sensing of alkaline phosphatase activity in living systems. Chem. Asian J. 2015, 10, 2444–2451.

80. Kim, T.I.; Kim, H.; Choi, Y.; Kim, Y. A fluorescent turn-on probe for the detection of alkaline phosphatase activity in living cells. Chem. Commun. 2011, 47, 9825–9827.

81. Zhang, H.; Xu, C.; Liu, J.; Li, X.; Guo, L.; Li, X. An enzyme-activatable probe with a self-immolative linker for rapid and sensitive alkaline phosphatase detection and cell imaging through a cascade reaction. Chem. Commun. 2015, 51, 703 1–7034.

82. He, Y.; Yu, J.; Hu, X.; Huang, S.; Cai, L.; Yang, L.; Zhang, H.; Jiang, Y.; Jia, Y.; Sun, H. An activity-based fluorescent pro be and its application for differentiating alkaline phosphatase activity in different cell lines. Chem. Commun. 2020, 56, 1 3323–13326.

83. Hou, X.; Yu, Q.; Zeng, F.; Ye, J.; Wu, S. A ratiometric fluorescent probe for in vivo tracking of alkaline phosphatase level variation resulting from drug-induced organ damage. J. Mater. Chem. B 2015, 3, 1042–1048.

84. Xiaohong Zhou; Yuren Jiang; Xiongjie Zhao; Yao Zhu; A New Two-Photon Ratiometric Fluorescent Probe for Detecting Alkaline Phosphatase in Living Cells. *Molecules* **2016**, *21*, 1619, 10.3390/molecules21121619.

85. Podder, A.; Senapati, S.; Maiti, P.; Kamalraj, D.; Jaffer, S.S.; Khatun, S.; Bhuniya, S. A ‘turn-on’ fluorescent probe for lys osomal phosphatase: A comparative study for labeling of cancer cells. J. Mater. Chem. B 2018, 6, 4514–4521.

86. Lu, Z.; Wu, J.; Liu, W.; Zhang, G.; Wang, P. A ratiometric fluorescent probe for quantification of alkaline phosphatase in living cells. RSC Adv. 2016, 6, 32046–32051.

87. Hu, Q.; Zeng, F.; Yu, C.; Wu, S. A fluorescent probe for alkaline phosphatase via excited state intramolecular proton tra nsfer. Sens. Actuators B Chem. 2015, 220, 720–726.

88. Liu, H.W.; Hu, X.X.; Zhu, L.; Li, K.; Rong, Q.; Yuan, L.; Zhang, X.B.; Tan, W. In vivo imaging of alkaline phosphatase in t umor-bearing mouse model by a promising near-infrared fluorescent probe. Talanta 2017, 175, 421–426.

89. Wang, W.X.; Jiang, W.L.; Guo, H.; Li, Y.; Li, C.Y. Real-time imaging of alkaline phosphatase activity of diabetes in mice via a near-infrared fluorescent probe. Chem. Commun. 2021, 57, 480–483.

90. Pang, X.; Li, Y.; Lu, Q.; Ni, Z.; Zhou, Z.; Xie, R.; Wu, C.; Li, H.; Zhang, Y. A turn-on near-infrared fluorescent probe for vi sualization of endogenous alkaline phosphatase activity in living cells and zebrafish. Analyst 2021, 146, 521–528.

91. Khatun, S.; Biswas, S.; Mahanta, A.K.; Joseph, M.M.; Vidyalekshmi, M.S.; Podder, A.; Maiti, P.; Maiti, K.K.; Bhuniya, S. Biocompatible fluorescent probe for detecting mitochondrial alkaline phosphatase activity in live cells. J. Photochem. P hotobiol. B Biol. 2020, 212, 112043.

92. Park, C.S.; Ha, T.H.; Kim, M.; Raja, N.; Yun, H.S.; Sung, M.J.; Kwon, O.S.; Yoon, H.; Lee, C.S. Fast and sensitive near-infrared fluorescent probes for ALP detection and 3d printed calcium phosphate scaffold imaging in vivo. Biosens. Bioel ectron. 2018, 105, 151–158.

93. Li, Y.; Xie, R.; Pang, X.; Zhou, Z.; Xu, H.; Gu, B.; Wu, C.; Li, H.; Zhang, Y. Aggregation-induced emission fluorescent pr obe for monitoring endogenous alkaline phosphatase in living cells. Talanta 2019, 205, 120143.

94. Li, J.; Huo, F.; Wen, Z.; Yin, C. A fluorescent turn-on probe based on isophorone for the rapid detection of alkaline phos phatase and its application in bioimaging. Spectrochim. Acta A Mol. Biomol. Spectrosc. 2019, 221, 117156.

95. Yangyang, Y.; Chen, Z.; Rizhao, P.; Shiwei, Z.; Shengtao, Y.; Yao, T.; Weilong, Z.; Liyue, W.; Weiping, Z.; Yufang, X.; et al. A ratiometric fluorescent probe for alkaline phosphatase with high sensitivity. Chin. Chem. Lett. 2020, 31, 125–128.

96. Gao, C.; Zang, S.; Nie, L.; Tian, Y.; Zhang, R.; Jing, J.; Zhang, X. A sensitive ratiometric fluorescent probe for quantitati ve detection and imaging of alkaline phosphatase in living cells. Anal. Chim. Acta 2019, 1066, 131–135.

97. Xu, L.; He, X.; Huang, Y.; Ma, P.; Jiang, Y.; Liu, X.; Tao, S.; Sun, Y.; Song, D.; Wang, X. A novel near-infrared fluorescen t probe for detecting intracellular alkaline phosphatase and imaging of living cells. J. Mater. Chem. B 2019, 7, 1284–12 91.

98. Lin, M.; Huang, J.; Zeng, F.; Wu, S. A fluorescent probe with aggregation-induced emission for detecting alkaline phosp hatase and cell imaging. Chem. Asian J. 2019, 14, 802–808.

99. Pandith, A.; Bhattarai, K.R.; Siddappa, R.K.G.; Chae, H.J.; Seo, Y.J. Novel fluorescent C2-symmetric sequential on-off-on switch for Cu2+ and pyrophosphate and its application in monitoring of endogenous alkaline phosphatase activity. S ens. Actuators B Chem. 2019, 282, 730–742.

100. Lim, E.K.; Keem, J.O.; Yun, H.S.; Jung, J.; Chung, B.H. Smart nanoprobes for the detection of alkaline phosphatase ac tivity during osteoblast differentiation. Chem. Commun. 2015, 51, 3270–3272.

101. Juan Ou-Yang; Chun-Yan Li; Yong-Fei Li; Bin Yang; Song-Jiao Li; An infinite coordination polymer nanoparticles-based near-infrared fluorescent probe with high photostability for endogenous alkaline phosphatase in vivo. *Sensors and Actu*

ators B: Chemical **2018**, *255*, 3355-3363, 10.1016/j.snb.2017.09.162.